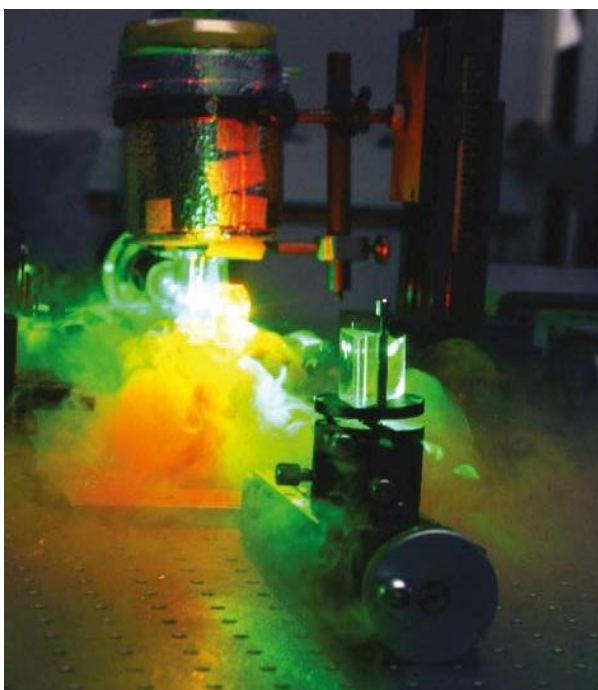


**В.Г. Беспалов, С.А. Козлов, С.Э. Путилин,
О.А. Смолянская**

**FEMTOSECOND OPTICS
AND FEMTOTECHNOLOGIES**



**Санкт-Петербург
2018**

МИНИСТЕРСТВО ОБРАЗОВАНИЯ И НАУКИ РОССИЙСКОЙ ФЕДЕРАЦИИ
УНИВЕРСИТЕТ ИТМО

В.Г. Беспалов, С.А. Козлов, С.Э. Путилин,
О.А. Смолянская

FEMTOSECOND OPTICS
AND FEMTOTECHNOLOGIES

РЕКОМЕНДОВАНО К ИСПОЛЬЗОВАНИЮ В УНИВЕРСИТЕТЕ
ИТМО по направлению подготовки бакалавров 12.03.03 и магистров
12.04.03 – «Фотоника и оптоинформатика».

 **УНИВЕРСИТЕТ ИТМО**

Санкт-Петербург

2018

Беспалов В.Г., Козлов С.А., Путилин С.Э., Смолянская О.А., Femtosecond optics and femtotechnologies. – СПб: Университет ИТМО, 2018. – 51 с.

Рецензенты: Яшин В.Е., доктор физ.-мат. наук, проф., нач. отделения АО«ГОИ им. С.И.Вавилова».

Анохина И.А., директор Лаборатории академического письма, Университет ИТМО

Аннотация.

В учебно-методическом пособии приводятся сведения о современном состоянии теоретических и экспериментальных исследований в области фемтосекундной оптики и об активно развивающихся в последние годы фемтотехнологиях. Пособие методически поддерживает дисциплину «Фемтосекундная оптика и фемтотехнологии» и состоит из следующих разделов «Theoretical methods of femtosecond optics», «Basics of femtosecond lasers», «Application of femtosecond lasers in medicine and biology», и «THz optics and spectroscopy».

Предназначено для студентов, обучающихся по направлению подготовки бакалавров 12.03.03 и магистров 12.04.03 – «Фотоника и оптоинформатика».

Университет ИТМО – ведущий вуз России в области информационных и фотонных технологий, один из немногих российских вузов, получивших в 2009 году статус национального исследовательского университета. С 2013 года Университет ИТМО – участник программы повышения конкурентоспособности российских университетов среди ведущих мировых научно-образовательных центров, известной как проект «5 в 100». Цель Университета ИТМО – становление исследовательского университета мирового уровня, предпринимательского по типу, ориентированного на интернационализацию всех направлений деятельности.

© Университет ИТМО, 2018

© Беспалов В.Г., Козлов С.А., Путилин С.Э., Смолянская О.А., 2018

Contents

Chapter 1. Theoretical methods of femtosecond optics	5
§1.1. Wave equation describing propagation of optical radiation in dielectrics ...	5
§1.2. Field equation for plane transversely homogeneous waves	6
§1.3 Field equation for unidirectional waves	8
§1.4. Nonlinear material equation describing the response of the dielectric media to the field of femtosecond pulses	9
§1.5. Examples of equations describing dynamic of radiation field in nonlinear dielectric media.....	11
§1.6. The field equations are generalization of envelope equations	12
§1.7. Normalizing the field dynamics equation.....	12
Chapter 2. Basics of femtosecond lasers.....	15
§2.1. Mode-locking, dispersion compensation.....	15
§2.2. Femtosecond lasers	16
§2.2.1. The dye laser with colliding pulses	16
§2.2.2. Titanium-sapphire laser.....	17
§2.2.3. The Yb-doped KYW laser.....	18
§2.2.4. The ring fiber laser	19
§2.3. Amplification of femtosecond pulses	20
§2.3.1. Principles of chirped-pulse amplification	20
§2.3.2. Regenerative amplifier	21
§2.3.3. Multi-pass amplifier	22
§2.4. Measurement of the duration and amplitude-phase femtosecond pulses... ..	23
§2.4.1. Autocorrelation methods.	23
§2.4.2. Methods for measuring the amplitude- phase characteristics of of pulse	24
Chapter 3. Application of femtosecond lasers in medicine and biology	28
§3.1. Dental Applications	30
§3.2. Ophthalmic Applications	33
§3.3. Neurosurgical Applications	34
§3.4. Subcellular Photodisruption.....	35
Chapter 4. THz optics and spectroscopy.....	38
§4.1. Methods of generating terahertz pulses with femtosecond lasers	38
§4.1.1. Introduction	38
§4.1.2. THz generation by photoconductive antennae I	38
§4.1.3. THz generation by optical rectification I	40
§4.1.4. THz generation using optical breakdown I.....	41
§4.1.5. Experimental apparatus	42
§4.1.6. THz generation by photoconductive antennae II	44
§4.1.7. THz generation by optical rectification II.....	44
§4.1.8. THz generation using optical breakdown II.....	46
§4.2. Time-resolved THz spectroscopy	46

Introduction

Femtosecond optics and femtotechnologies are a fascinating research area in optics and modern innovative technologies, which can be used in information and communication technologies, environmental engineering and life sciences (medicine, biology, chemistry), to name a few applications. The university discipline of femtosecond optics and femtotechnologies is aimed at forming the corresponding competences of a Master student in the related field.

This textbook is one of the resources of the discipline «Femtosecond optics and femtotechnologies» and consists of the following sections «Theoretical methods of femtosecond optics», «Basics of femtosecond lasers», «Application of femtosecond lasers in medicine and biology», «THz optics and spectroscopy». The discipline «Femtosecond optics and technology» is part of the Master's course in the «Photonics and Optoinformatics» based on modern theoretical concepts and experimental methods of modern optics of ultrashort pulses and technologies based on them. It does not only provide knowledge and hard skills required by the state educational standard, but contributes to developing higher level skills within the strategy and ideology of the science area, as well as the thinking skills of master students.

Chapter 1. Theoretical methods of femtosecond optics

This Chapter discusses the methods of theoretically describing the propagation of pulses with durations of less than 10^{-12} seconds. In the domain of such short pulses, optical materials may not destroy even at very high radiation intensities, at least, within the femtosecond pulse. With high-intensity femtosecond radiation we can easily observe some phenomena that are almost never encountered in the field of longer pulses due to the destruction of optical materials. For example, the phenomenon of spectral supercontinuum generation in the field of femtosecond pulses is observed in almost all transparent materials [1], while the traditional methods of theoretically describing nonlinear propagation of laser pulses usually assume radiation as being quasi-monochromatic. It is clear that the equations of the field dynamics of femtosecond radiation should take into account the possibility of strong broadening of the pulse spectrum in a nonlinear medium. This chapter discusses such equations of field dynamics, which allow describing the strong changes in the radiation spectrum. It is shown that such equations should include, as a special case, the equations of dynamics of quasi-monochromatic waves that are quite well-known and are still often used in nonlinear optics of ultrashort pulses. The Chapter provides some practical exercises.

§1.1. Wave equation describing propagation of optical radiation in dielectrics

In classical physics, space and time dynamics of electromagnetic field is described by Maxwell's equations

$$\left\{ \begin{array}{l} \nabla \times \vec{E} = -\frac{\partial \vec{B}}{\partial t} \\ \nabla \times \vec{H} = \vec{j} + \frac{\partial \vec{D}}{\partial t} \\ \nabla \vec{D} = \rho \\ \nabla \vec{B} = 0, \end{array} \right. \quad (1)$$

where \vec{E} and \vec{H} are the electric and magnetic field strengths, \vec{D} is the electric displacement, \vec{B} is the magnetic flux density, ρ is the volume charge density, \vec{j} is the electric current density. Equations (1) are written in SI units.

Two vector and two scalar equations (1) are equivalent to eight scalar equations. At the same time, the system contains five vectors and one scalar unknown function. They are equivalent to fifteen scalar functions. Therefore, Maxwell's equations must be supplemented by material equations, which for dielectric media have the form

$$\vec{j} = 0, \rho = 0 \quad (2a)$$

$$\vec{B} = \mu_0 \vec{H} \quad (2b)$$

$$\vec{D} = \vec{D}(\vec{E}). \quad (2c)$$

The equation (2a) indicates that there are no free charges in the medium (it is a dielectric), (2b) indicates that the medium is non-magnetic and (2c) indicates that the electric induction is not determined by the magnetic field.

Our choice of dielectrics as the media for studying light propagation is due to the wide application of transparent dielectric media in femtosecond optics. But it is also important to note that the theoretical methods we consider below are suitable for studying the media of other nature, for instance for semiconductors.

We apply vector operation $\nabla \times$ to the left and right sides of the first Maxwell's equation, use the second equation and also take into account expressions (2a) for dielectrics. As the result we obtain the equation

$$\nabla \times (\nabla \times \vec{E}) = -\frac{\partial}{\partial t} \nabla \times \vec{B} = \mu_0 \frac{\partial^2 \vec{D}}{\partial t^2}. \quad (3)$$

Thus, for electromagnetic radiation in dielectrics we obtain the wave equation in SI units in the form of

$$\nabla \times \nabla \times \vec{E} + \mu_0 \frac{\partial^2 \vec{D}}{\partial t^2} = 0. \quad (4)$$

Exercise 1. Derive the wave equation in Gaussian units in the form of

$$\nabla \times \nabla \times \vec{E} + \frac{1}{c^2} \frac{\partial^2 \vec{D}}{\partial t^2} = 0. \quad (5)$$

The first term in wave equations (4) and (5) describes the diffraction of radiation, and the second one describes the response of the matter to the action of the force of electromagnetic field.

Using the wave equation, we will consider below the features of propagation dynamics of the simplest type of wave as a plane transversely homogeneous wave.

§1.2. Field equation for plane transversely homogeneous waves

In the approximation of plane transversely homogeneous wave, the wave equation takes a form much simpler than (4) or (5)

$$\frac{\partial^2 \vec{E}}{\partial z^2} - \frac{1}{c^2} \frac{\partial^2 \vec{D}}{\partial t^2} = 0, \quad (6)$$

where $\vec{D} = \vec{E} + 4\pi\vec{P}$ (Gaussian units), $\vec{D} = \epsilon_0\vec{E} + \vec{P}$ (SI units). We neglect the diffraction of light in this approximation.

It is convenient to consider the polarization of the medium in the form of $\vec{P} = \vec{P}_{\text{lin}} + \vec{P}_{\text{nl}}$, where \vec{P}_{lin} is linear and \vec{P}_{nl} is nonlinear functionals of \vec{E} . Then the equation (6) takes the form of

$$\frac{\partial^2 \vec{E}}{\partial z^2} - \frac{1}{c^2} \frac{\partial^2 \vec{E}}{\partial t^2} = \frac{4\pi}{c^2} \frac{\partial^2 \vec{P}_{\text{lin}}}{\partial t^2} + \frac{4\pi}{c^2} \frac{\partial^2 \vec{P}_{\text{nl}}}{\partial t^2}. \quad (7)$$

Let us consider two basic scenarios of field dynamics of electromagnetic wave, the methods of their analysis making them different.

1. Low-intensity radiation: value P_{nl} can be neglected.

We note two useful methods for accounting for light dispersion in a linear dielectric medium.

a) The inertia of the polarization response of a homogeneous isotropic medium is described by the functional

$$\vec{P}_{\text{lin}} = \int_{-\infty}^t \chi(t-t') E(t') dt'. \quad (8)$$

b) The dispersion of the linear refractive index of a homogeneous isotropic medium is described by the relation

$$n^2(\omega) = N_0^2 + (2cN_0a)\omega^2 + (2cN_0a_1)\omega^4 + \dots - (2cN_0b)\frac{1}{\omega^2} - (2cN_0b_1)\frac{1}{\omega^4} - \dots, \quad (9)$$

where $A \equiv 2cN_0a$, $A_1 \equiv 2cN_0a_1$, $B \equiv 2cN_0b$, $B_1 \equiv 2cN_0b_1$ are phenomenological constants describing the particular optical medium.

Comment: for dielectric susceptibility $\chi(\omega) = \int_{-\infty}^{\infty} \chi(t) e^{-i\omega t} dt$ relation

$n^2(\omega) = \varepsilon(\omega) = 1 + 4\pi\chi(\omega)$ is valid, where $\varepsilon(\omega)$ is dielectric permittivity.

The dispersion relation (9) is the basis for the wave equation

$$\frac{\partial^2 \vec{E}}{\partial z^2} - \frac{N_0^2}{c^2} \frac{\partial^2 \vec{E}}{\partial t^2} = -\frac{2N_0}{c} a \frac{\partial^4 \vec{E}}{\partial t^4} + \frac{2N_0}{c} a_1 \frac{\partial^6 \vec{E}}{\partial t^6} - \dots + \frac{2N_0}{c} b \vec{E} - \frac{2N_0}{c} b_1 \int_{-\infty}^t dt' \int_{-\infty}^{t'} Edt'' + \dots, \quad (10)$$

where $-\frac{2N_0}{c} a = \frac{A}{c^2}$, $\frac{2N_0}{c} a_1 = \frac{A_1}{c^2}$, $\frac{2N_0}{c} b = \frac{B}{c^2}$. It is easy to verify this by finding a partial solution of (10) in the form of a monochromatic wave

$$\vec{E} = \frac{1}{2} \vec{E}_\omega e^{i(kz - \omega t)} + c.c.$$

Exercise 2. Let us substitute the solution in the form of a monochromatic wave into the wave equation. We obtain:

$$\frac{1}{2} \vec{E}_\omega (-k^2) e^{i(kz - \omega t)} - \frac{N_0^2}{c^2} \frac{1}{2} \vec{E}_\omega (-\omega^2) e^{i(kz - \omega t)} = -\frac{2N_0}{c} a \frac{1}{2} \vec{E}_\omega (\omega^4) e^{i(kz - \omega t)} + \frac{2N_0}{c} a_1 \frac{1}{2} \vec{E}_\omega (-\omega^6) e^{i(kz - \omega t)} - \dots + \frac{2N_0}{c} b \frac{1}{2} \vec{E}_\omega e^{i(kz - \omega t)} - \frac{2N_0}{c} b_1 \frac{1}{2} \vec{E}_\omega \left(\frac{1}{-\omega^2} \right) e^{i(kz - \omega t)} + \dots$$

Dividing both sides of equation by $\frac{1}{2} \vec{E}_\omega e^{i(kz - \omega t)}$, we obtain

$$-k^2 + \frac{N_0^2}{c^2} \omega^2 = -\frac{2N_0}{c} a \omega^4 - \frac{2N_0}{c} a_1 \omega^6 - \dots + \frac{2N_0}{c} b + \frac{2N_0}{c} b_1 \left(\frac{1}{\omega^2} \right) + \dots,$$

where $k(\omega) = n(\omega) \cdot \frac{\omega}{c}$, $n^2(\omega) = \frac{c^2}{\omega^2} k^2(\omega)$.

As the result, we obtain

$$n^2(\omega) = N_0^2 + 2N_0 c a \omega^2 + 2N_0 c a_1 \omega^4 + \dots - 2N_0 c b \left(\frac{1}{\omega^2} \right) - 2N_0 c b_1 \left(\frac{1}{\omega^4} \right) - \dots$$

Q.E.D.

Conclusion: This section demonstrates the principle of constructing linear equations describing field dynamics of radiation with a broad spectrum in a dispersive medium.

2. High-intensity radiation: value P_{nl} cannot be neglected.

Equation (7) with regard to (10) can be written in the form of

$$\frac{\partial^2 \vec{E}}{\partial z^2} - \frac{N_0^2}{c^2} \frac{\partial^2 \vec{E}}{\partial t^2} = -\frac{2N_0}{c} a \frac{\partial^4 \vec{E}}{\partial t^4} + \frac{2N_0}{c} a_1 \frac{\partial^6 \vec{E}}{\partial t^6} + \frac{4\pi}{c^2} \frac{\partial^2 \vec{P}_{nl}}{\partial t^2}. \quad (11)$$

Equation (11) describes the propagation of radiation in a nonlinear optical medium in both directions.

§1.3 Field equation for unidirectional waves

For the analysis of the dynamics of light pulses propagating in only one direction of the z axis (e.g. positive) it is advisable to switch to new variables:

$$\begin{aligned} z' &= z \\ \tau &= t - \frac{N_0}{c} z \end{aligned} \quad (12)$$

$$E(z, t) \rightarrow E(z', \tau).$$

It is useful to remember the rules of differentiation of functions when passing to new variables

$$\begin{aligned} \frac{\partial E}{\partial z} &= \frac{\partial E}{\partial z'} \frac{\partial z'}{\partial z} + \frac{\partial E}{\partial \tau} \frac{\partial \tau}{\partial z} = \frac{\partial E}{\partial z'} - \frac{N_0}{c} \frac{\partial E}{\partial \tau} \\ \frac{\partial E}{\partial t} &= \frac{\partial E}{\partial z'} \frac{\partial z'}{\partial t} + \frac{\partial E}{\partial \tau} \frac{\partial \tau}{\partial t} = \frac{\partial E}{\partial \tau}. \end{aligned}$$

Exercise 3. Determination of the second derivatives of the wave equation in new variables. We obtain

$$\frac{\partial^2 E}{\partial z^2} = \frac{\partial^2 E}{\partial z'^2} \frac{\partial z'}{\partial z} + \frac{\partial^2 E}{\partial z' \partial \tau} \frac{\partial \tau}{\partial z} - \frac{N_0}{c} \frac{\partial^2 E}{\partial \tau \partial z'} \frac{\partial z'}{\partial z} - \frac{N_0}{c} \frac{\partial^2 E}{\partial \tau^2} \frac{\partial \tau}{\partial z} = \frac{\partial^2 E}{\partial z'^2} - \frac{2N_0}{c} \frac{\partial^2 E}{\partial z' \partial \tau} + \frac{N_0^2}{c^2} \frac{\partial^2 E}{\partial \tau^2},$$

$$\frac{\partial^2 E}{\partial t^2} = \frac{\partial^2 E}{\partial z' \partial \tau} \frac{\partial z'}{\partial t} + \frac{\partial^2 E}{\partial \tau^2} \frac{\partial \tau}{\partial t} = \frac{\partial^2 E}{\partial \tau^2}.$$

Then equation (11) in new variables takes the form of

$$\frac{\partial^2 \vec{E}}{\partial z'^2} - \frac{2N_0}{c} \frac{\partial^2 \vec{E}}{\partial z' \partial \tau} = -\frac{2N_0}{c} a \frac{\partial^4 \vec{E}}{\partial \tau^4} + \frac{2N_0}{c} b \vec{E} + \frac{4\pi}{c^2} \frac{\partial^2 \vec{P}_{nl}}{\partial \tau^2}. \quad (13)$$

Using approximation of the slowly varying field profile, i.e. assuming that the change in the profile of the pulse field along the length compared to the central wavelength is small, the term $\frac{\partial^2 \vec{E}}{\partial z'^2}$ is neglected. After integrating the equation (13)

we obtain

$$\frac{\partial \vec{E}}{\partial z'} - a \frac{\partial^3 \vec{E}}{\partial \tau^3} + b \int_{-\infty}^{\tau} \vec{E} d\tau' + \frac{2\pi}{cN_0} \frac{\partial \vec{P}_{nl}}{\partial \tau} = 0. \quad (14)$$

Truncated (with the first derivative of z) equation (14) is the equation describing unidirectional field dynamics of radiation with a wide spectrum in a nonlinear dielectric.

§1.4. Nonlinear material equation describing the response of the dielectric media to the field of femtosecond pulses

The nonlinear polarization response of an isotropic medium in the classical theory is usually written in the form

$$\frac{\partial^2 \vec{P}}{\partial t^2} + \frac{2}{T} \frac{\partial \vec{P}}{\partial t} + \omega_0^2 \vec{P} + k\vec{P}^3 + \dots = \alpha \vec{E}, \quad (15)$$

here $\vec{P} = N\vec{p}$, \vec{p} is the dipole moment of the structural unit of matter (atom in gas, elementary cell in solid), N is the concentration of atoms or molecules.

Comment: For an anisotropic medium $\frac{2}{T}$, ω_0^2 , k are not scalar but tensor dimension; quadratic term in the field E appears in the equation.

In dielectric usually $\omega_0^2 \gg \omega^2$, that is why

$$\frac{\partial^2 P}{\partial t^2} \approx \omega^2 P \ll \omega_0^2 P. \quad (16)$$

Taking into account (16), it is possible to write (15) in the form

$$\vec{P} = \frac{\alpha}{\omega_0^2} \vec{E} - \frac{1}{\omega_0^2} \frac{\partial^2 \vec{P}}{\partial t^2} - \frac{2}{T\omega_0^2} \frac{\partial \vec{P}}{\partial t} - \frac{k\vec{P}^3}{\omega_0^2} - \dots, \quad (17)$$

where all terms beginning with the second term in the right side of the equation are much smaller than the first.

We solve the equation (17) by iteration method. In the zero iteration we have

$$\vec{P}^{(0)} = \frac{\alpha}{\omega_0^2} \vec{E}. \quad (18)$$

In the next iteration

$$\vec{P}^{(1)} = \frac{\alpha}{\omega_0^2} \vec{E} - \frac{\alpha}{\omega_0^4} \frac{\partial^2 \vec{E}}{\partial t^2} - \frac{2\alpha}{T\omega_0^4} \frac{\partial \vec{E}}{\partial t} - \frac{k\alpha}{\omega_0^4} \vec{E}^3. \quad (19)$$

Equation (19) describes the inertia and nonlinearity of the polarization response of the medium.

Then the wave equation

$$\frac{\partial^2 \vec{E}}{\partial z^2} - \frac{1}{c^2} \frac{\partial^2 \vec{E}}{\partial t^2} - \frac{4\pi}{c^2} \frac{\partial^2 \vec{P}^{(1)}}{\partial t^2} = 0 \quad (20)$$

takes the form

$$\frac{\partial^2 \vec{E}}{\partial z^2} - \frac{1 + 4\pi \frac{\alpha}{\omega_0^2}}{c^2} \frac{\partial^2 \vec{E}}{\partial t^2} + \frac{4\pi\alpha}{\omega_0^4 c^2} \frac{\partial^4 \vec{E}}{\partial t^4} + \frac{8\pi\alpha}{T\omega_0^4} \frac{\partial^3 \vec{E}}{\partial t^3} + \frac{k\alpha}{\omega_0^4} \frac{\partial^3 \vec{E}}{\partial t^2} = 0. \quad (21)$$

It is appropriate to compare it with the equation earlier obtained by another method (13).

Comment: Besides the electronic response, in a mathematical model of dielectric it is often appropriate to take into account the vibrational response of the lattice in the optical field

$$\vec{P}_\Sigma = \vec{P}_e + \vec{P}_v. \quad (22)$$

We consider it linear:

$$\frac{\partial^2 \vec{P}_v}{\partial t^2} + \omega_{0v}^2 \vec{P}_v = \alpha_v \vec{E}. \quad (23)$$

We neglected the lattice absorption of matter in (23) for simplicity.

It is usually $\omega^2 \gg \omega_{0v}^2$, then

$$\frac{\partial^2 \vec{P}_v}{\partial t^2} = \alpha_v \vec{E}. \quad (24)$$

It is the reason for the term $\frac{4\pi\alpha_v}{c^2} \vec{E}$ to appear in the wave equation (21). Please compare it with the earlier obtained equation (13).

Conclusion: The simple classical theory of dispersion will show that:

1. Linearized equation of field dynamics coincides with the previously derived equation for an arbitrary dispersion law.
2. The expression for the nonlinear part of the polarization response of the medium is of the form $\vec{P}_{nl} = \chi E^3 +$ small corrections (taking into account dispersion and higher field order).

It can be shown that for the classical theory to yield the same result as the quantum theory (in the description of the inertia of the nonlinear part of a polarization of medium), a modification is required [2]:

$$\left\{ \begin{array}{l} \frac{\partial^2 \vec{P}_{nl}}{\partial t^2} + \frac{2}{T_{e1}} \frac{\partial \vec{P}_{nl}}{\partial t} + \omega_{e1}^2 \vec{P}_{nl} + k \vec{P}_{nl}^3 - (R_e + R_v) \vec{E} = 0 \\ \frac{\partial^2 R_e}{\partial t^2} + \frac{2}{T_{e2}} \frac{\partial R_e}{\partial t} + \omega_{e2}^2 R_e = \gamma_e E \\ \frac{\partial^2 R_v}{\partial t^2} + \frac{2}{T_v} \frac{\partial R_v}{\partial t} + \omega_v^2 R_v = \gamma_v E, \end{array} \right. \quad (25)$$

where the second equation describes electronic vibrations of dielectric medium, the third one - molecular vibrations (they describe stimulated Raman scattering).

§1.5. Examples of equations describing the dynamics of radiation field in nonlinear dielectric media

1. Modified Korteweg-de Vries equation

$$\frac{\partial E}{\partial z} - a \frac{\partial^3 E}{\partial \tau^3} + g E^2 \frac{\partial E}{\partial \tau} = 0 \quad (26)$$

describes the self-action of a linearly polarized wave in a dielectric medium with normal group dispersion.

2. In equation

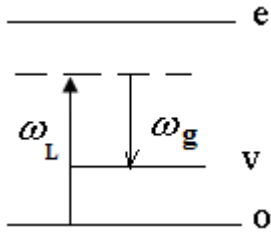
$$\frac{\partial E}{\partial z} - a \frac{\partial^3 E}{\partial \tau^3} + b \int_{-\infty}^{\tau} E d\tau' + g E^2 \frac{\partial E}{\partial \tau} = 0 \quad (27)$$

dispersion law of refractive index is defined more exactly, which allows us to describe an anomalous group dispersion of the medium.

Exercise 4. Obtain the dispersion relations for equations (26) and (27).

$$3. \left\{ \begin{array}{l} \frac{\partial E}{\partial z} - a \frac{\partial^3 E}{\partial \tau^3} + b \int_{-\infty}^{\tau} E d\tau' + g E^2 \frac{\partial E}{\partial \tau} + \frac{\partial}{\partial \tau} (R_v E) = 0 \\ \frac{\partial^2 R_v}{\partial t^2} + \frac{2}{T_v} \frac{\partial R_v}{\partial t} + \omega_v^2 R_v = \gamma_v \vec{E}. \end{array} \right. \quad (28)$$

Stimulated Raman scattering is also taken into account in the system of equations (28).



§1.6. The field equations are a generalization of envelope equations

Exercise 5. Use the substitution of the form

$$E(z,t) = \frac{1}{2} E(z,t) e^{i(k_0 z - \omega_0 t)} + k.c. \quad (29)$$

to the equation of field dynamics

$$\frac{\partial E}{\partial z} + \frac{N_0}{c} \frac{\partial E}{\partial t} - a \frac{\partial^3 E}{\partial \tau^3} + g E^2 \frac{\partial E}{\partial \tau} = 0. \quad (30)$$

to obtain dispersion relation

a) for linearized equation (30)

$$i k_0 - \frac{N_0}{c} i \omega_0 - a (i \omega_0)^3 = 0, \quad k_0 = \frac{N_0}{c} \omega_0 + a \omega_0^3, \quad n = N_0 + a c \omega_0^2$$

b) for nonlinear equation (30) taking into consideration that

$$E^3 = \frac{1}{8} (E_0^3 e^{3i(k_0 z - \omega_0 t)} + |E_0^2| E_0 e^{i(k_0 z - \omega_0 t)} + k.c.), \quad n(\omega) = N_0 + a c \omega_0^2 + \frac{g |E_0^2| \omega_0}{4}.$$

In the approximation of slowly varying envelopes, the equation of the envelope dynamics should be obtained in the form [3]

$$\begin{aligned} \frac{\partial E}{\partial z} + \frac{1}{V} \frac{\partial E}{\partial t} + i \frac{\beta_2}{2} \frac{\partial^2 E}{\partial \tau^2} - \frac{\beta_3}{6} \frac{\partial^3 E}{\partial \tau^3} - i \gamma_1 |E^2| E + \gamma_2 \frac{\partial}{\partial t} (|E^2| E) - \\ - \left(i \gamma_1 E^3 - \gamma_2 E^2 \frac{\partial E}{\partial t} \right) e^{2i(k_0 z - \omega_0 t)} = 0, \end{aligned} \quad (31)$$

where

$$V = \left(\frac{\partial k}{\partial \omega} \right)_{\omega_0}^{-1}, \quad \beta_n = \left(\frac{\partial^n k}{\partial \omega^n} \right)_{\omega_0}, \quad k = \frac{N_0}{c} \omega + a \omega^3, \quad \gamma_1 = \frac{g \omega_0}{4}, \quad \gamma_2 = \frac{g}{4}, \quad k_0 = \frac{N_0}{c} \omega_0 + a \omega_0^3.$$

$$\frac{1}{V} = \frac{N_0}{c} + 3a \omega_0^2, \quad \beta_2 = 6a \omega_0, \quad \beta_3 = 6a.$$

§1.7. Normalizing the field dynamics equation

Let us carry out a typical normalization procedure, for example, for the equation

$$\frac{\partial E}{\partial z} - a \frac{\partial^3 E}{\partial \tau^3} + g E^2 \frac{\partial E}{\partial \tau} = 0. \quad (32)$$

Normalizing is also determined by boundary conditions. Let us assume that

$$E(0,t) = E_0 e^{-\frac{t^2}{\tau^2}} \sin(\omega_0 t). \quad (33)$$

1. Let us pass on to new variables $\hat{E} = \frac{E}{E_0}$, $\hat{\tau} = \omega_0 \tau$. Then

$$\frac{\partial \hat{E}}{\partial z} - a \omega_0^3 \frac{\partial^3 \hat{E}}{\partial \tau^3} + g \omega_0 E_0^2 \hat{E}^2 \frac{\partial \hat{E}}{\partial \tau} = 0.$$

2. It is also appropriate to introduce $\hat{z} = a \omega_0^3 z$. Then

$$\begin{cases} \frac{\partial \hat{E}}{\partial \hat{z}} - a \frac{\partial^3 \hat{E}}{\partial \hat{\tau}^3} + \frac{g E_0^2}{a \omega_0^2} \hat{E}^2 \frac{\partial \hat{E}}{\partial \hat{\tau}} = 0, G = \frac{g E_0^2}{a \omega_0^2} \\ \hat{E}(0, \hat{\tau}) = e^{-\frac{\hat{\tau}^2}{\tau^2}} \sin(\hat{\tau}). \end{cases} \quad (34)$$

Conclusion:

1. The integral parameter G is introduced, thus, it is possible to evaluate the nature of the process:

the case $G \ll 1$ describes linear field propagation in the medium;

the case $G \gg 1$ describes nonlinear field propagation in the medium.

2. Grid of numerical calculation is normalized to unity.

3. One numerical calculation allows us to describe processes for many situations.

In this Chapter, we have considered the methods for deriving equations of field dynamics of femtosecond pulses. We discussed the appropriate approximations that allowed us to get them. These equations make it possible to describe nonlinear propagation of radiation in optical media, the spectrum of which can become very wide in the process of interaction with the matter. These equations contain, as a limiting case, some equations of nonlinear dynamics of quasi-monochromatic pulses well-known in nonlinear optics.

For many results of theoretical research of the features of femtosecond nonlinear optics received by means of the equations deduced above please refer to papers [4-10] below, to name a few examples.

REFERENCES

1. Gouairona A., Mysyrowicz A. Femtosecond filamentation in transparent media. // Physics Reports, 2007, 441, pp. 47 – 189.
2. Kozlov S.A., Samartsev V.V. Fundamentals of femtosecond optics. – Woodhead Publishing Limited. 2013. – 272 p.
3. Agrawal G.P. Nonlinear Fiber Optics. – 5nd ed. Academic Press. New York. 2013. – 631 p.
4. Buyanovskaya E.M., Kniazev M.A., Kozlov S.A., Sukhorukov A.A. Harmonic generation enhancement due to interaction of few-cycle light pulses in

- nonlinear dielectric coating on a mirror. // *Physics Letters A*, IET - 2017, Vol. 381, No. 43, pp. 3714-3721.
5. Kapoyko Y.A., Drozdov A.A., Kozlov S.A., Zhang Xi-C. Evolution of few-cycle pulses in nonlinear dispersive media: Velocity of the center of mass and root-mean-square duration. – *Physical Review A*. 2016. V. 94. N. 3. P. 033803.
 6. Tcypkin A.N., Putilin S.E., Melnik M.V., Makarov E.A., Bepalov V.G., Kozlov S.A. Generation of high-intensity spectral supercontinuum of more than two octaves in a water jet. – *Applied Optics*. 2016. V. 55. N. 29. P. 8390-8394.
 7. Dolgaleva K., Materikina D.V., Boyd R.W., Kozlov S.A. Prediction of an extremely large nonlinear refractive index for crystals at terahertz frequencies. – *Physical Review A*. 2015. V. 92. N. 2. P. 023809.
 8. Drozdov A.A., Kozlov S.A., Sukhorukov A.A., Kivshar Yu.S. Self-phase modulation and frequency generation with few-cycle optical pulses in nonlinear dispersive media // *Phys. Rev. A*. 2012. V. 86. N 5. P. 053822-10.
 9. Ezerskaya A.A., Ivanov D.V., Kozlov S.A., Kivshar Yu.S. Spectral Approach in the Analysis of Pulsed Terahertz Radiation // *J Infrared Milli. Terahz. Waves*. 2012. V. 33. N 9. P. 926–942.
 10. Thomson, C. Leburn, D. Reid *Ultrafast Nonlinear Optics*. – Springer International Publishing. 2013. – 377 p.

Chapter 2. Basics of femtosecond lasers

§2.1. Mode-locking, dispersion compensation

Longitudinal cavity mode-locking is a method of generating ultrashort laser pulses. The pulse length is typically much less than the time of double resonator passing, and pulse-repetition frequency (from several dozen MHz to several hundred GHz) is determined by the time of double resonator passing, when the mode-locking is continuous.

Modulator of the intercavity losses is mounted in the laser resonator for mode-locking. A modulator of losses is used for gathering the laser radiation in short pulses near the minimum of loss of the modulator with a period equal to double passing of resonator.

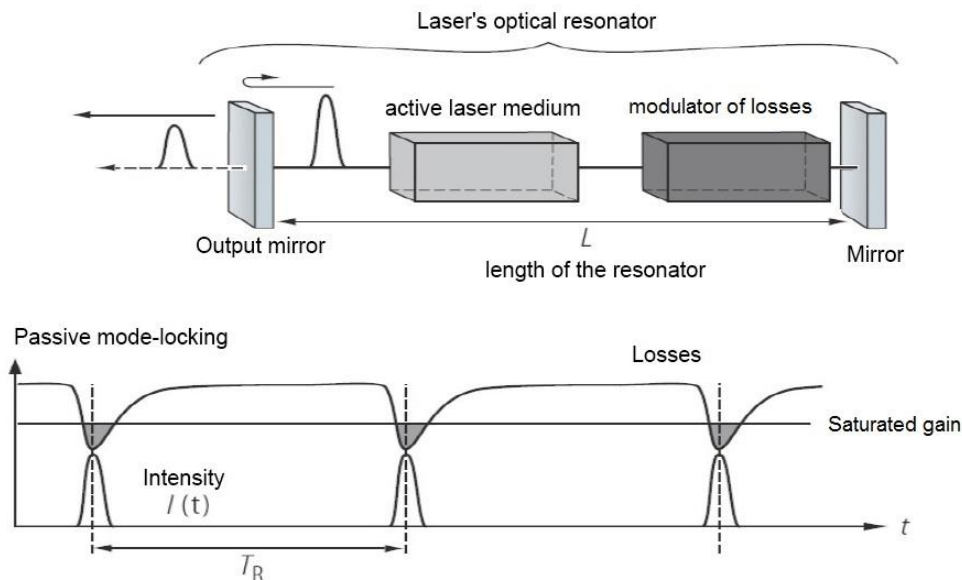


Fig. 2.1. The diagram of the laser resonator and the intensity dependence on time with passive mode-locking

Passive mode-locking is used to produce femtosecond pulses. Modulator of losses produces a loss of intra-cavity radiation, which is relatively high for low intensities, but quite low for high intensities. Thus, a short pulse causes small modulation losses. Due to the high radiation intensity in the main peak of the pulse, the modulator of losses makes fewer losses than in pulse wing with low intensity. This leads to a loss modulation with quick initial absorption. In fact, the pulse circulating in the resonator saturates laser gain to a level just sufficient to compensate for the losses in the pulse itself, while the rest of the low-intensity radiation is subjected to absorption to a greater extent than the gain, and disappears during the following cavity round trips.

The question is in how passive mode-locking starts. Theoretically, it starts from the usual noise fluctuations in the laser. One of the noise spikes is strong

enough to significantly reduce losses in the noise modulator, and therefore it is amplified more than the weak one when passing the resonator. This leads to the fact that the strongest noise spike continues to reduce its loss in the loss modulator and continues to grow until it reaches a steady state where a stable pulse sequence is formed.

The dispersion of the active medium and other components of the resonator is undesirable in femtosecond lasers. In nature, all transparent substances have a normal (positive) dispersion. It is advisable to make the dispersion of resonator equal to zero to produce bandwidth-limited pulses, therefore dispersion compensator should have abnormal (negative) dispersion. The prismatic dispersion compensator has this property. It consists of a pair of prisms disposed at a distance opposite each other. The passage of this device by the light is equivalent to the passage of a structure with abnormal dispersion, and dispersion depends on the distance between the prisms and the properties of the prism material.

Chirped mirrors are also used for dispersion compensation.

§2.2. Femtosecond lasers

§2.2.1. Dye laser with colliding pulses

Dye lasers use a solution of an organic dye as the active medium. They were used for the generation of picosecond and femtosecond light pulses before the titanium-sapphire lasers appeared.

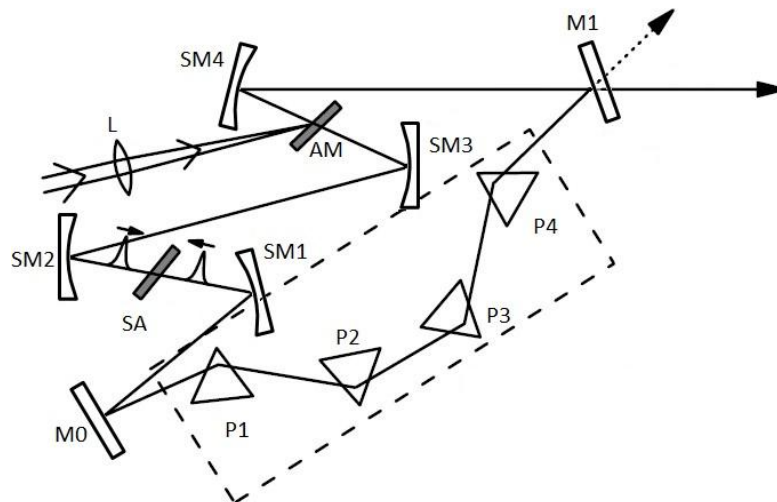


Fig. 2.2. Optical scheme of a jet dye laser with colliding pulses

First optical pulse length of less than 100 fs was obtained in 1981 [1] by using a jet dye laser with a ring resonator and colliding pulses in a jet saturable absorber (Fig. 2.2.). For several years their scheme (colliding pulse mode locking-CPM laser) remained the most common for generating femtosecond pulses. A laser resonator consisted of four spherical mirrors (SM1-SM4), a flat mirror M0 and an output coupler M1. The saturable absorber is used as a modulator of losses. A jet of dye solution of rhodamine 6G is used as the active medium (AM), and a jet of dye solution of DODCI - as a saturable absorber (SA).

The saturable absorber shortens the front part of the pulse, and the active medium shortens the back part by the amplification in saturation. The combination of the saturation of absorption and the amplification shortens the pulse down to the final steady state.

The laser generates pulses with duration of up to 65 fs.

Using prismatic dispersion compensator consisting of four prisms (P1-P4) allowed the authors [2] to obtain pulses with duration of 27 fs. The pulse duration of 33 fs was obtained in the linear resonator geometry with dispersion compensation and without a colliding pulse mode. [2a]

§2.2.2. Titanium-sapphire laser

Femtosecond lasers based on titanium sapphire crystals generate in the visible and near-infrared range. Titanium sapphire crystals have spectral bands of gain that are among the widest (600-1100 nm).

Absorption in corundum with titanium is characterized by a wide band in the range of 400-600 nm, which is a superposition of two bands with the maxima at 490 nm and at 550 nm.

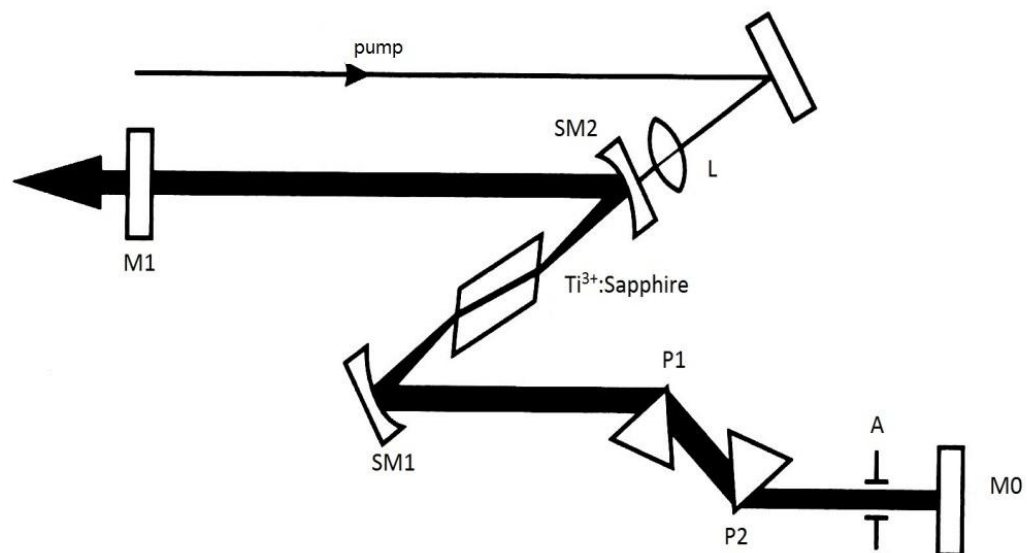


Fig. 2.3. Optical scheme of a titanium-sapphire laser

Kerr lens is used as a modulator of losses. A dynamical Kerr lens forms due to self-focusing in the propagation of radiation in a titanium-sapphire crystal. Its relaxation time is of a few femtoseconds. The distance between the spherical mirrors SM1 and SM2 (Fig.2.3.) is settled with regard to dynamic Kerr lens to maximize the quality of the resonator in the femtosecond mode.

Optical scheme of femtosecond laser based on titanium-sapphire crystal is shown in figure 2.17. Pump radiation is reflected from the mirror and with a short-focus lens L is focused to the titanium-sapphire crystal through a spherical, dichroic mirror SM2.

Spherical mirrors SM1-SM2 form the resonator mode with small caustic in the active medium. The laser resonator is formed by a system of mirrors SM1-

SM2, M0-M1. Dispersion compensator consisting of two fused silica prisms P1-P2 is mounted inside the laser resonator for group speed dispersion compensation.

First titanium sapphire laser was used for the generation of femtosecond pulses in [3]. The optical scheme of the laser is shown in Fig 2.3. The pulse duration at the output of the laser was of 60fs, and of 45fs after an external prismatic compressor. Three years later, with the same geometry of the resonator, pulses with duration of 8.5 fs were obtained [4]. In [5] the pulse duration of 5 fs was obtained.

Since the value of the Kerr lens is determined by the intensity of the intracavity radiation, for a continuous femtosecond generation, the pump laser must have a high power stability with respect to time. Femtosecond generation in titanium-sapphire crystals can be obtained by laser pumping in a continuous mode with the aid of a gas argon laser or the second harmonic of Nd:YAG and Nd:YLF solid-state lasers with diode pumping. In recent years, direct diode pumping of a femtosecond titanium-sapphire laser has been reported [6]

§2.2.3. Yb-doped KYW laser

Yb-doped laser materials are well suited for building simple and robust diode-pumped femtosecond lasers delivering output powers in the Watt range. Yb:YAG and Yb:glass are the most common representatives of this class of materials and have been applied in lasers for ultrashort pulses [7,8]. In general, Yb-doped laser crystals and glasses exhibit broad emission spectra supporting pulse durations below 100 fs. Relatively broad absorption bands with large cross sections can be pumped by InGaAs laser diodes. Emission cross sections are large enough, so that relatively high gain is provided and in the case of mode-locked operation good stability against Q-switching can be expected because of the low saturation fluence [7]. Fluorescence lifetimes are generally longer than in Nd-doped hosts. The small quantum defect enhances the overall efficiency and reduces the thermal load. On the other hand, a disadvantage of Yb-doped laser materials is their quasi-three-level nature. As a result, they reabsorb a part of the emitted laser light. A high pump intensity and a good overlap of pump and resonator mode over the whole length of the laser medium are required to saturate this loss mechanism.

The operation of femtosecond lasers using Yb:KGW and, very recently, Yb:KYW was shown in [10] and [11]. The former was passively mode-locked by a saturable absorber mirror (SESAM), the latter was Kerr-lens mode-locked. Both were pumped by broad stripe diodes. Here we present what is to our knowledge the first laser using Yb:KYW with a SESAM for a self-starting mode-locking process and a novel tapered diode laser as high brightness pump source. The shortest pulse duration was achieved in [11] (71 fs). Relatively simple beam shaping optics is sufficient due to the excellent beam quality of the TDL. The astigmatic emission of the tapered diode laser is formed by an aspherical and a cylindrical lens (Fig. 2.4). The nearly collimated pump beam is then focused by an $f = 62.8$ -mm spherical lens through one of the folding mirrors of the Z-folded resonator. The 3-mm thick Yb:KYW crystal is used under Brewster angle for polarization almost parallel to the m-crystallo-optic axis, which turned out to be optimum for achieving

maximum output power and stable mode-locking. At a doping level of 5at.% Yb about 98% of the incident 1.1 W of pump power are absorbed. Although the Yb:KYW crystal is not actively cooled, no thermal problems occurred. Two Brewster-cut SF10 prisms are used for dispersion compensation in the arm containing the output coupler. The SESAM, serving as a passive mode-locker, is placed at the other end of the resonator where an additional waist is formed by a curved mirror.

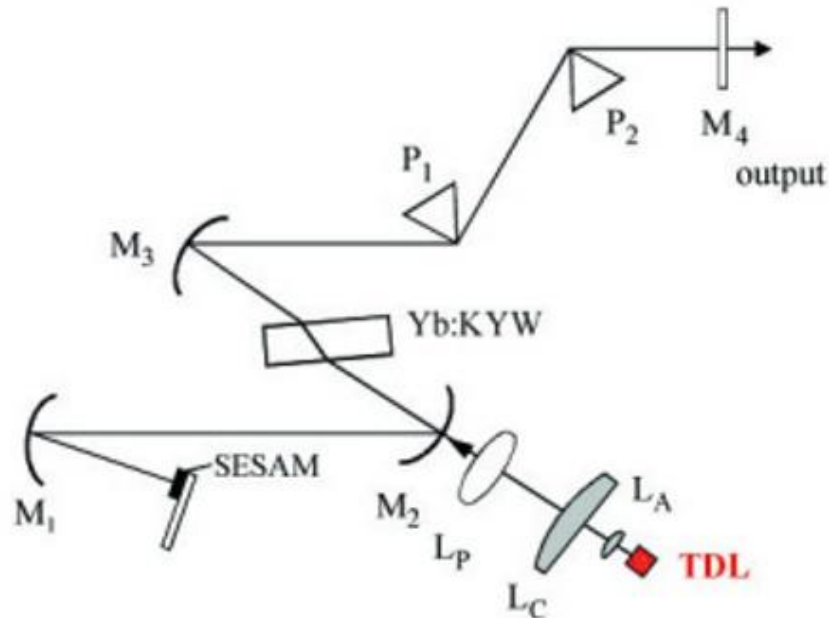


Fig. 2.4. Setup of the femtosecond Yb:KYW laser: SESAM - semiconductor saturable absorber mirror; M_1 - focusing mirror ($r = 100$ to 150 mm); M_2 , M_3 - folding mirrors ($r = 100$ mm), P_1 , P_2 - SF10 Brewster prisms; M_4 - output coupler ($T_{\text{output coupler}} = 1$ to 5%); Yb:KYW - 3-mm-long, 5 at% Yb^{3+} -doped crystal; TDL - tapered diode laser; L_A - aspherical lens; L_C - cylindrical lens; L_P - focusing lens

§2.2.4. Ring fiber laser

The first generation of femtosecond pulses using a fiber laser was implemented in 1990 [13]. The minimum duration of lasers on a fiber with nonlinear compression is less than 10 fs [14] The most common femtosecond fiber lasers are Er and Yb lasers which generate, respectively, at a wavelength of 1.55 microns and 1.05 microns.

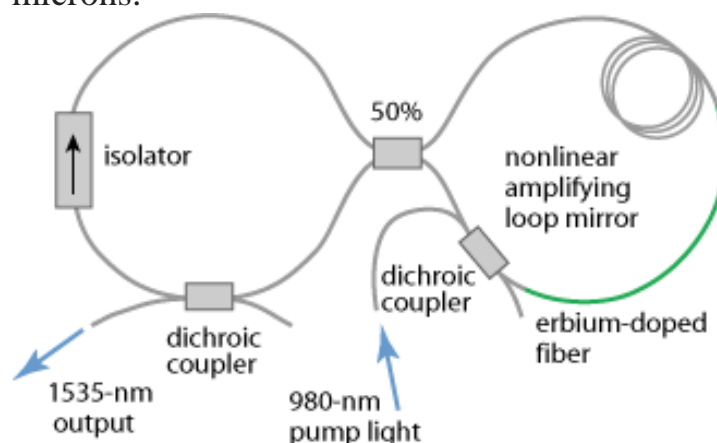


Fig. 2.5. Diagram of a ring fiber laser

Both linear and non-linear changes in the polarization of the radiation propagating through the optical fiber are the basis for the generation of femtosecond pulse for most fiber lasers. They use a birefringent optical fiber on which radiation propagates with two linear orthogonal polarizations with almost equal low losses.

But the effect of the phase self-modulation may lead to a rotation of the polarization ellipse in isotropic optical fibers. The nonlinear polarization rotation together with the polarizer is used in a fiber laser as a modulator of losses. The process of the rotation of polarization in optical fiber at high powers of radiation is shown in Fig 2.6.

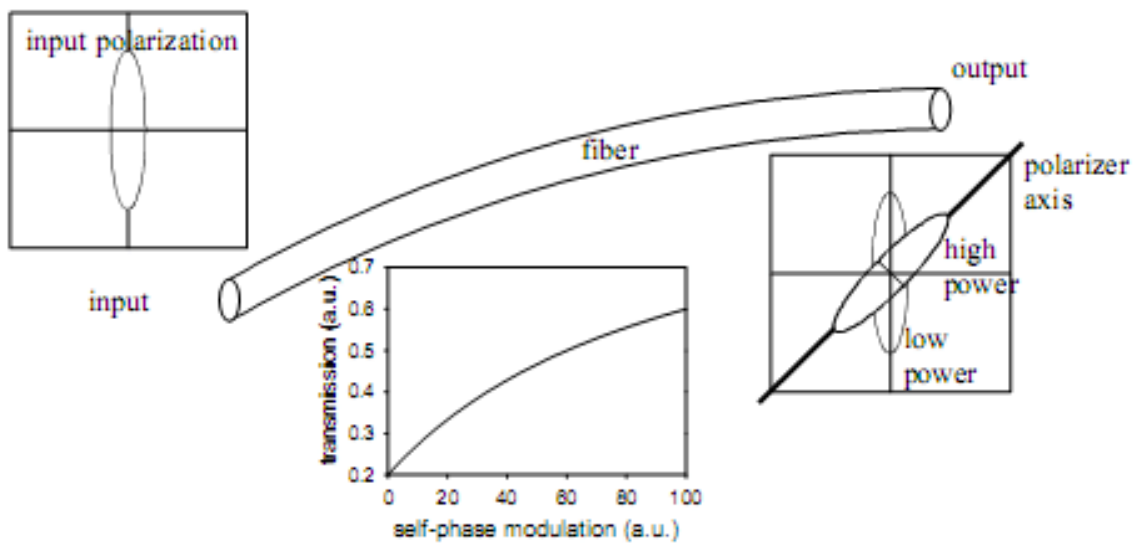


Fig. 2.6. Principle of the rotation of elliptical polarization in optical fiber and its application for an optical switch

§2.3. Amplification of femtosecond pulses

§2.3.1. Principles of chirped-pulse amplification

Significant progress in increasing the peak power was achieved using the method of chirped pulse amplification proposed in mid 1980s [15] (Fig. 2.7.).

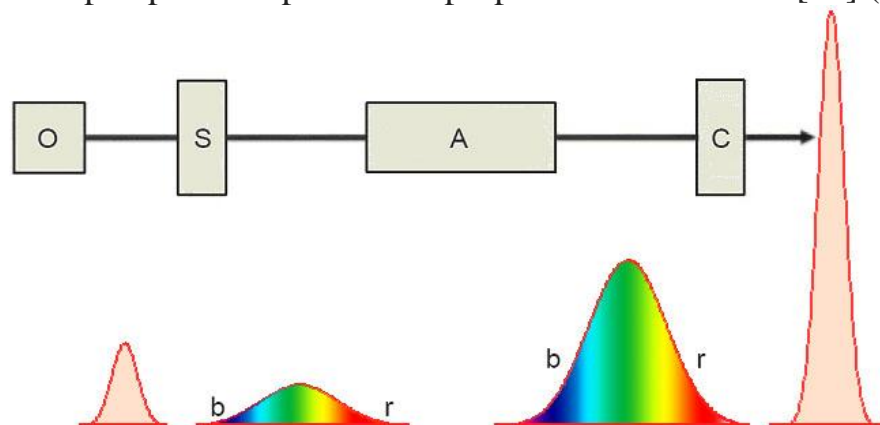


Fig. 2.7. Diagram showing the principle of chirped pulse amplification. The pulse of the generator (O) stretches in the stretcher (S) so that the red (r) components was ahead of the blue

one(b). The peak intensity decreases. Then the stretched pulse is amplified in the amplifier (A) and compressed in the compressor (C)

The essence of the method of chirped pulse amplification is in that the amplified pulse is passed through delay line with a large group speed dispersion (stretcher) in which it becomes linearly chirped, and its duration is greatly increased up to 10^5 times (up to several nanoseconds). Its peak power is similarly reduced. Such chirped pulse can be effectively amplified without damaging the optical elements of the amplifier. Then the pulse repetition rate is reduced by Pockels cell. The pulse is amplified. After amplification, the pulse is passed through the other delay line having the same group speed dispersion, but with the opposite sign (compressor). As a result, the chirp is compensated, and the amplified pulse gets a duration close to the original. A scheme of a gain chirped pulse is shown in Figure 2.6.

Titanium-sapphire [15] and glass doped with neodymium ions [16] and their hybrids are the most effective media for high-power laser systems with a chirped pulse amplification.

Currently, the most powerful laser system based on titanium-sapphire crystal [15] generates pulses with duration of 19,4 fs, pulse energy 83J and the peak power of 4,2 PW. Alternative powerful hybrid laser system based on titanium-sapphire crystal and glass doped with neodymium [17] generates pulses of 440 fs, pulse energy of 660J, and peak power of 1.5 PW.

A stretcher [18] is designed for extension of pulses in time. It has a positive dispersion and consists of a pair of diffraction gratings, between which there is a telescopic system with increasing -1 . The stretcher has a positive dispersion until the distance between the grating and the lens is less than the lens focal length.

A compressor [19] having a negative dispersion and consisting of a pair of diffraction gratings and a corner reflector is used for the pulse compression in time. It compensates for the dispersion of the amplified pulse.

§2.3.2. Regenerative amplifier

The regenerative amplifier is designed for significant amplification of femtosecond pulses (up to 10^7). Regenerative amplification is the most effective way to transmit power from the amplifier to femtosecond pulses. Fig. 2.8. shows an optical scheme of a regenerative amplifier. Femtosecond pulses from the oscillator (laser) pass the stretcher and a Faraday isolator, get to the polarizer P1, pass Pockels cell PC1 and are reflected from the mirror M1. If Pockels cell is not alive, the light will not change the polarization state and will not fall into the amplifier reflected from the mirrors M1 and from the polarizer P1. By applying the appropriate voltage to the Pockels cell, the polarization state of pulse will change to the orthogonal and the pulse will be trapped in a resonator of the regenerative amplifier. The amplifier resonator consists of two flat mirrors, M1, M2 and two spherical mirrors SM1, SM2. The pump radiation is reflected from the mirror Mp and focuses to the active medium by a lens L. Q-switched lasers with pulse

duration in the dozens or hundreds of nanoseconds are used for pumping. The injected pulse is amplified in a resonator until it reaches saturation (it usually takes 15-30 passes), and then to Pockels cell. PC2 appropriate voltage is applied; after passing the Pockels cell, the pulse reflected from the mirror M2 and passing Pockels cell PC2 again, changes the polarization state to the orthogonal and is reflected from the polarizer P2; the amplified pulse is ejected from the regenerative amplifier and comes to the next amplifier or compressor.

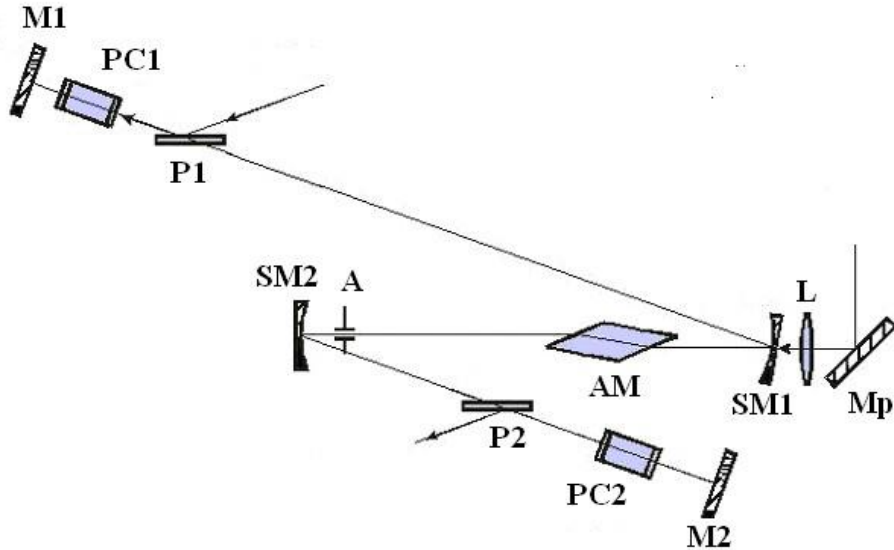


Fig. 2.8. Optical scheme of a regenerative amplifier

Special electronic circuits for synchronization and control of Pockels cells are used to synchronize the pump pulse, Pockels cells and femtosecond pulse sequence are generated by the master-oscillator laser.

§ 2.3.3. Multi-pass amplifier

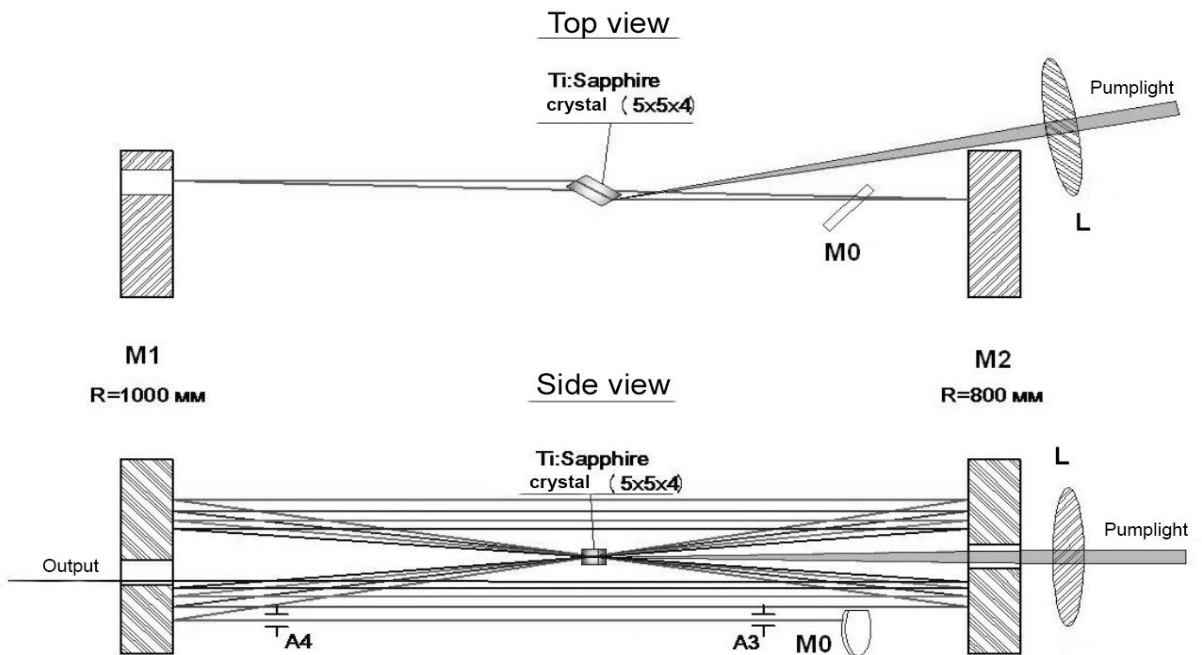


Fig. 2.9. Optical scheme of multipass telescopic amplifier

Multipass amplifiers are also intended for significant amplification of femtosecond pulses. They are typically used for 8 to 10 passes through the active medium for the first amplification stage and from 4 to 8 passages for the second stage. A scheme of a multipass optical amplifier is shown in Fig. 2.9. Femtosecond pulses from the master-oscillator laser pass the stretcher, a Faraday isolator and Pockels cell where the selection of a single pulse takes place. The selected pulse passes through the mirror M0 to the multi-pass amplifier input. A telescopic multipass amplifier consists of two spherical mirrors M1, M2, and the active medium which is located near the focus of the two mirrors. Curve radii of the mirrors M2 and M1 are different, thus, the beam diameter is reduced after each pass through the active medium, and the diameter of the waist in the active medium increases. This makes it possible to get the maximum amplification of the pulse without a risk of damaging the active element. A spherical mirror M1 has a hole in the center for ejecting the amplified radiation. The pumping radiation is focused to the active medium by a lens L and passes close to a cut of mirror M2.

§2.4. Measurement of the duration and amplitude-phase of femtosecond pulses.

§2.4.1. Autocorrelation methods.

The measurement of the duration of the light pulse with optical methods is based on the transference of temporary measurement to spatial. If there are two time dependent functions $F(t)$ and $F'(t)$, and one of them is known, for example, $F'(t)$, then the measurement function $G(\tau)$, defined as

$$G(\tau) = \int_{-\infty}^{+\infty} F'(t)F(t - \tau)dt \quad (2.4.1)$$

Makes it easy to identify the second unknown function $F(t)$. $G(t)$ is the correlation function of the first order. Unfortunately, the test pulse described by the function $F'(t)$, cannot be synthesized for short time intervals, and therefore, autocorrelation function is used for the real measurement. In this case, a single laser pulse is split into two (one with a time delay) - $F(t)$ and $F(t-\tau)$ and they interfere and create the autocorrelation function [20-21].

The autocorrelation function may be experimentally obtained by multiphoton processes (such as using a two-photon absorption photodiode or a second harmonic generation).

For the case of collinear SHG, the measured intensity may be represented in the form

$$I_2(\tau) = \int \left| \{E(t)\exp[i\omega t + \Phi(t)] + E(t-\tau)\exp[i\omega(t-\tau) + \Phi(t-\tau)]\}^2 \right|^2 dt \quad (2.4.2)$$

For the autocorrelation function of the second order (see equation 2.4.2.) signal when $\tau = 0$ is

$$I_2(\tau=0) = 2^4 \int E^4(t)dt \quad (2.4.3.)$$

$$\text{and when } \tau \rightarrow \infty = 2 \int E^4(t) dt \quad (2.4.4.)$$

so, in this case, the contrast is $16/2 = 8$. At present, the optical scheme shown in Fig. 2.10 is typically used for determining the autocorrelation function of the second order (for lasers using high pulse repetition rate).

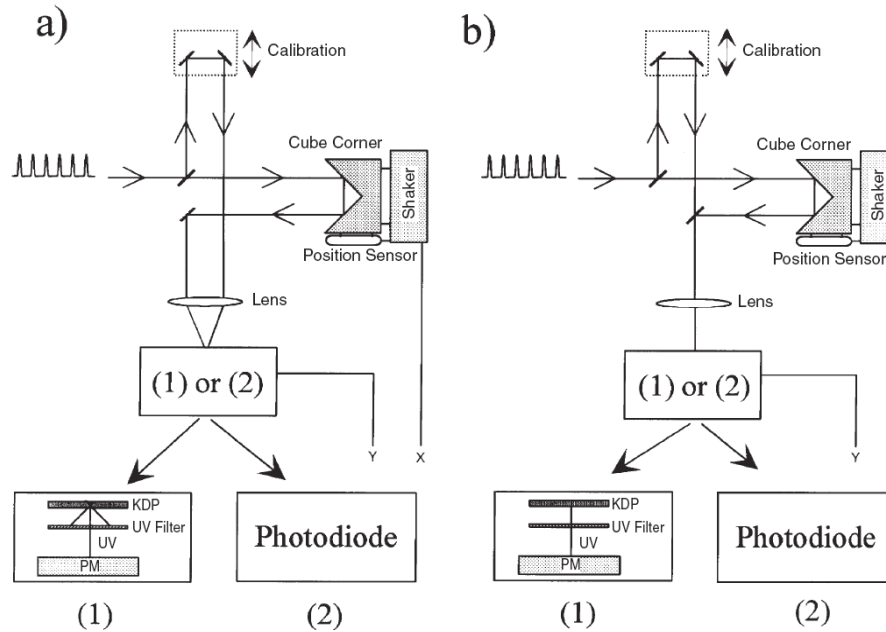


Fig. 2.10. Optical scheme for measuring the autocorrelation function of the second order. a) non-collinear SHG b) collinear SHG

§2.4.2. Methods for measuring the amplitude-phase characteristics of the pulse

The measurement of the autocorrelation function and the spectrum does not provide any information about the temporal shape of femtosecond pulse. For example, a chirp can be detected, but it cannot be determined if it is contained in the pulse. To determine the time waveform, it is necessary to measure its amplitude and phase. There are several methods for this. The most well-known is FROG (Frequency Resolved Optical Gating) [22].

Let us consider FROG based on non-collinear SHG (Figure 2.10a (1)). The analyzed ultrashort pulse is split by beam splitter into two parts, which fall to the nonlinear crystal at a small angle. Noncollinear SHG appears only when both pulses cross in space and time simultaneously. Noncollinear second-harmonic radiation is focused on the slit of the spectrometer. Spectral decomposition of the pulse by spectrometer is in a plane orthogonal to the plane formed by beams participating in SHG. We obtain a two-dimensional image of the investigated pulse decomposed both by the wavelength and in time (Figure 2.11.a) on the CCD matrix in the spectral plane of the spectrometer.

This FROG image does not contain any phase. Frog algorithm is used to determine the phase. Figure 2.11.b shows FROG image reconstruction, carried out using the above algorithm. The lower row on the left shows the reconstructed

temporal pulse shape and the phase dependence on time (Figure 2.11.c), the right side shows the reconstructed pulse spectrum and the phase dependence on wavelength (Figure 2.11.d).

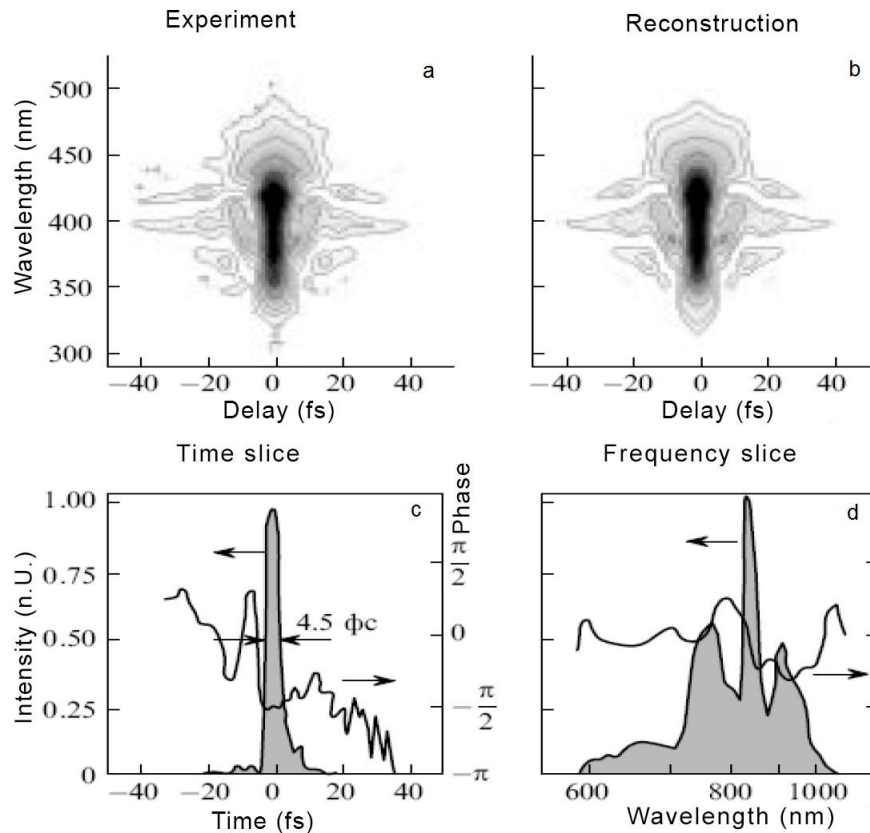


Fig. 2.11. An example of registering a 4.5-fs pulse using FROG based on non-collinear SHG [23]

REFERENCES

1. Fork R. L., Greene B. I., Shank, C.V. Generation of optical pulses shorter than 0.1 psec by colliding pulse mode locking, *Appl. Phys. Lett.*, 1981, V. 38, p. 671-672.
2. A. Valdvanis J. A., Fork R. L., Gordon J. P., Generation of optical pulses as short as 27 femtoseconds directly from a laser balancing self-phase modulation, group-velocity dispersion, saturable absorption, and saturable gain *Opt. Lett.*, 1985, V. 10, p. 131-133.
3. Spence D. E., Kean P. N., Sibbett W., 60-fsec pulse generation from a self-mode-locked Ti:sapphire laser *Opt. Lett.*, 1991, V. 16, p. 42-44.
4. Zhou J., Taft G., Huang C., Murnane M. M., Kapteyn H. C., Christov I. P., Pulse evolution in a broad-bandwidth Ti:sapphire laser, *Opt. Lett.*, 1994, V. 19, p. 1149-1151.
5. Ell R., Morgner U., Kärtner F. X., Fujimoto J. G., Ippen E. P., Scheuer V., Angelow G., Tschudi T., Lederer M. J., Boiko A., Luther-Davies B., Generation of 5-fs pulses and octave-spanning spectra directly from a Ti:sapphire laser, *Opt. Lett.*, 2001, V. 26, p. 373-375.

6. Gürel, K., Wittwer, V. J., Hoffmann, M., Saraceno, C. J., Hakobyan, S., Resan, B., Südmeyer, T. . Green-diode-pumped femtosecond Ti: Sapphire laser with up to 450 mW average power. *Optics express*, 2015, V. 23(23), p. 30043-30048.
7. J. Aus der Au, G. J. Spühler, T. Südmeyer, R. Paschotta, R. Hävel, M. Moser, S. Erhard, M. Karszewski, A. Giesen, and U. Keller, 16.2-W average power from a diode-pumped femtosecond Yb:YAG thin disk laser, *Opt. Lett.*, 2000, V. 25, p. 859–861.
8. V. Petrov, U. Griebner, D. Ehrt, and W. Seeber, Femtosecond self mode locking of Yb:fluoride phosphate glass laser, *Opt. Lett.*, 1997, V. 22, p. 408–410.
9. C. Hönniger, R. Paschotta, F. Morier-Genoud, M. Moser, and U. Keller, Q-switching stability limits of continuous-wave passive mode locking, *J. Opt. Soc. Am.*, 1999, V. B16, p. 46–56.
10. F. Brunner, G. J. Spühler, J. Aus der Au, L. Krainer, F. Morier-Genoud, R. Paschotta, N. Lichtenstein, S. Weiss, C. Harder, A. A. Lagatsky, A. Abdolvand, N. V. Kuleshov, and U. Keller, Diode-pumped femtosecond Yb:KGd(WO₄)₂ laser with 1.1-W average power, *Opt. Lett.*, 2000, V. 25, p. 1119–1121.
11. H. Liu, J. Nees, and G. Mourou, Diode-pumped Kerr-lens mode-locked Yb:KYW laser, in *OSA Trends in Optics and Photonics (TOPS) Vol.56, Conference on Lasers and Electro-Optics (CLEO 2001), Technical Digest (Optical Society of America, Washington DC,2001)*, p. 30–31.
12. Fermann M. E., Hofer M., Haberl F., Craig-Ryan, S. P., Femtosecond fiber laser, *Electron. Lett.*, 1990, 26: 1737 – 1738.
13. Sell A., Krauss G., Scheu R., Huber R., Leitenstorfer A., 8-fs pulses from a compact Er: fiber system: quantitative modeling and experimental implementation, *Opt. Exp.*, 2009, V. 17, p. 10
14. Strickland D., Mourou G. Compression of amplified chirped optical pulses // *Opt. Comm.* 1985. V. 56. P. 219–221.
15. Sung, J. H., Lee, H. W., Yoo, J. Y., Yoon, J. W., Lee, C. W., Yang, J. M., Son Y. J., Jang Y. H., Lee S. K., Nam, C. H. 4.2 PW, 20 fs Ti: sapphire laser at 0.1 Hz. *Opt. Lett.*, 2017, V. 42(11), p. 2058-2061.
16. Yamakawa, K., Shiraga, H., Kato, Y. & Barty, C. P. J. Prepulse-free 30-TW, 1-ps Nd:glass laser. *Opt. Lett.*, 1991, V. 16, p. 1593-1595
17. Perry M. D., Pennington D., Stuart B. C., Tietbohl G., Britten J. A., Brown C., Herman S., Golick B., Kartz M., Miller J., Powell H. T., Vergino M., Yanovsky V., Petawatt laser pulses, *Opt. Lett.*, 1999, V. 24, p. 160-162
18. Martinez O. E., Gordon J. P., Fork R. L., Negative group-velocity dispersion using refraction, *J. Opt. Soc. Am. A*, 1984, V. 1, p. 1003-1006.
19. Treacy E.B. Optical pulse compression with diffraction gratings. // *IEEE J. Quantum. Electron.*- 1969.- Vol. 5.- N .- p. 454-458
20. Fontaine, W. Rudolph: Ultrafast diagnostics, *Rev. Phys. Appl.*, 1987, v. 22, p. 1605-1611.
21. J.-C. Diels, W. Rudolph: Ultrashort Laser Pulse Phenomenon: Fundamentals, Techniques and Applications on a Femtosecond Time Scale, Academic Press, Boston (1996)

22. Kane D., Trebino R., Characterization of arbitrary femtosecond pulses using frequency-resolved optical gating, IEEE J. Quantum Electron., 1993, V. 29, p. 571-579
23. Baltuska A., Pshenichnikov M. S., Weirsmas, D. A., Second-harmonic generation frequency-resolved optical gating in the single-cycle regime, IEEE J. Quant. Electron., 1999, V. 35, p. 459-478.

Chapter 3. Application of femtosecond lasers in medicine and biology

INTRODUCTION

Femtosecond technology, with its ultrashort light pulses, is an innovative laser technology that can be used for multiple applications, e.g., in industrial manufacturing, information and communication technologies, environmental technology and life sciences (medicine, biology, chemistry). This chapter concentrates on the use of ultrashort pulses as a tool for ultraprecise material removal in manufacturing and medical therapy, as well as a tool for metrology and for X-ray production.

The most striking feature of the new technology is the extreme shortness of the laser pulses ranging from about 10 fs (10^{-14} s) to 10 ps (10^{-11} s) [1, 2]. To give an example: within 100 fs, light travels only as far as a fraction of the diameter of a human hair. For comparison: within one second, light can circle the earth about 7.5 times. Another predominant feature of ultrashort pulses is their extremely high intensity. During the pulse a power level of hundreds of gigawatts is achieved, that is, as much as all the power plants of Germany deliver together. For example, at a pulse width of 100 fs and a focal area of $100 \mu\text{m}^2$ the pulse energy of 1mJ yields an intensity value of 10^{16}W/cm^2 .

Biological tissue has a relatively low linear absorption coefficient especially in the mid-infrared region, where most femtosecond lasers emit (Fig. 3.1) [3]. As a consequence, plasma formation has a different origin and time history from those in metals, where the direct linear absorption plays a major role for generating the first free electrons of the plasma. In low-absorbing and low scattering material optical breakdown can thus occur not only at the surface of the tissue but also inside the bulk. Here, different phenomena take place, such as optical-induced breakdown on a surface, cavitation and bubble development on the free surface, multiphoton absorption, plasma creation and propagation, generation and movement of very high air pressure.

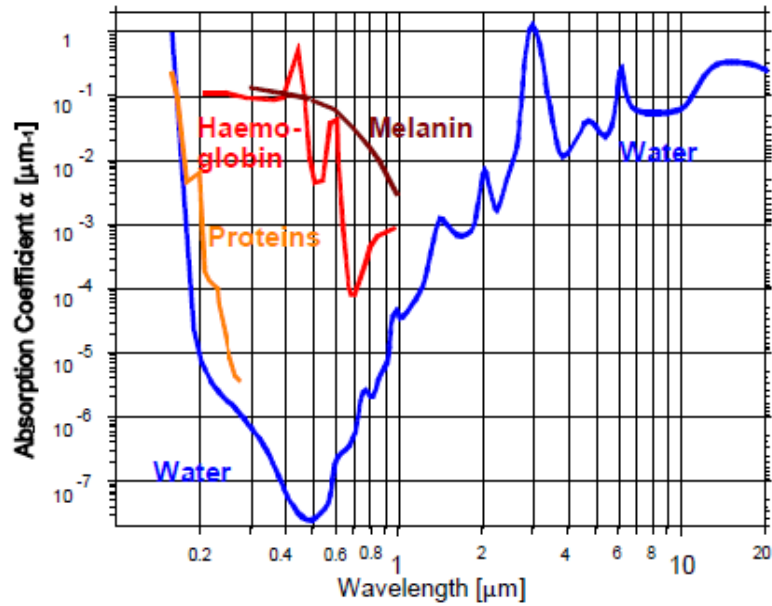


Fig. 3.1. Absorption of different chromophores of biological tissue. In the infrared region, where most of the femtosecond lasers operate, the average penetration depth $1/a$ is within the range of a few millimeter (Data from [3])

In water, the effect might be caused by a local increase of the temperature. If one roughly estimates the volume of all filaments to be in the range of $3 \cdot 10^{-7} \text{ cm}^3$ (10 filaments with 1mm in length and $3 \text{ }\mu\text{m}$ in diameter) and 50% of the laser pulse energy is converted into heat, the temperature would increase by 38K. This would cause a change in the index of refraction by 0.005. On the timescale of several microseconds, cavitation can be observed (Figure 3.2). Due to the intensity distribution of the focused laser beam, a cylindrical shape of the bubble develops. Because of the surface tension, the bubble collapses faster at smaller radii of curvature, which turns the bubble into a sphere during collapse. After $3 \text{ }\mu\text{s}$, the bubble has blown up again in a second cycle. Now its shape is like that of a small disc, perpendicular to the original elongation of the cylinder. After $7.5 \text{ }\mu\text{s}$ the bubble has finally collapsed to a size of approximately $6 \text{ }\mu\text{m}$ in diameter and begins to rise to the surface.

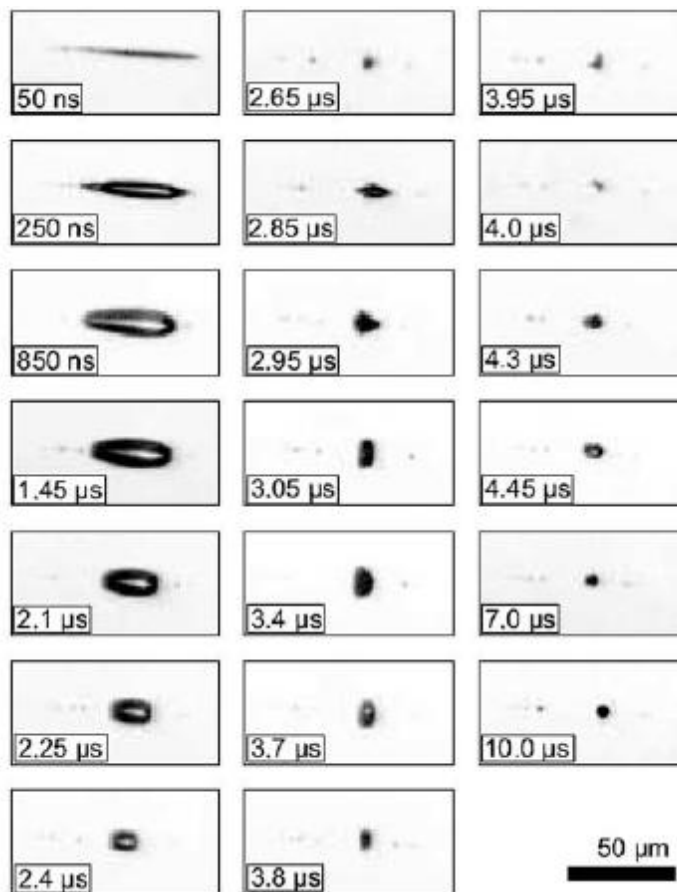


Fig. 3.2. Sequence of laser-induced cavitation bubbles 50 ns to 10 μ s after optical breakdown at a pulse energy of 5 μ J and the pulse duration of 175 fs. The laser beam entered from the right

§3.1. Dental Applications

In dentistry the specific interactions between ultrashort laser pulses and enamel/dentin of a tooth or ceramic restoration materials are advantageous due to minimal collateral damage. The femtosecond laser beam can be used as a tool to remove either decayed enamel/dentin – also named caries – or as a tool to remove ceramic from a bulk until the shape of an all-ceramic restoration is left. Therefore, a completely new caries therapy and an innovative way to manufacture all ceramic dental restorations are possible if femtosecond laser devices emitting pulses with a high energy and repetition rate are available [4, 5]. Although the latter has not become a commercial possibility yet, basic research has to be done to evaluate the interactions between lasers and materials depending on various laser parameters. This strategy enables a specific development of dental femtosecond laser sources based on optimized laser parameters. Additionally, the high demand of an intraorally application of a femtosecond laser beam can be met by developing a dental handpiece.

In extracted human third molars, cavities are generated with a CPA (chirped pulse amplification) Ti:sapphire femtosecond laser [6]. The cavities are ablated by

scanning the focused laser pulses (100 μm) with a computer-controlled x-y galvanometer scanner over the tooth surface at a scan velocity of 200mm/s. The SEM in Fig. 3a-c shows the result created at a wavelength of 780 nm, a pulse duration of 700 fs, a pulse energy of 100 μJ and a pulse repetition rate of 5 kHz. The extremely precise tetragonal cavity (Fig. 3.3a) is located within healthy dentin. It has a lateral dimension of 2mm \times 2mm and a depth of approximately 1.4 mm. The two white rectangles are enlarged (Fig. 3b-c). The roughness of the cavity bottom (Fig. 3.3b) is of the order of 5 μm to 10 μm and thus facilitates the direct adhesion of most filling materials without any etching gel. The cavity margin is sharp and free of chippings, the cavity wall (Fig. 3.3c) is extremely steep and clean, the cavity bottom shows no smear layer and open dentinal tubuli, taken together these are ideal conditions for a perfect filling. A second cavity has been created within healthy and carious dentin with the carious lesion being located in the top left corner at the tip of the white arrow (Fig. 3.4a). Obviously, carious substance is removed more efficiently than healthy dentin. The enlargement (Fig. 4b) shows a very clean surface after laser exposure, thus proving that all carious substance has been completely removed in that area. Again, the cavity wall is extremely steep and precise. A third cavity has been located within carious enamel at the most typical location of a carious lesion that is on top of the chewing surfaces (Fig. 3.5a).

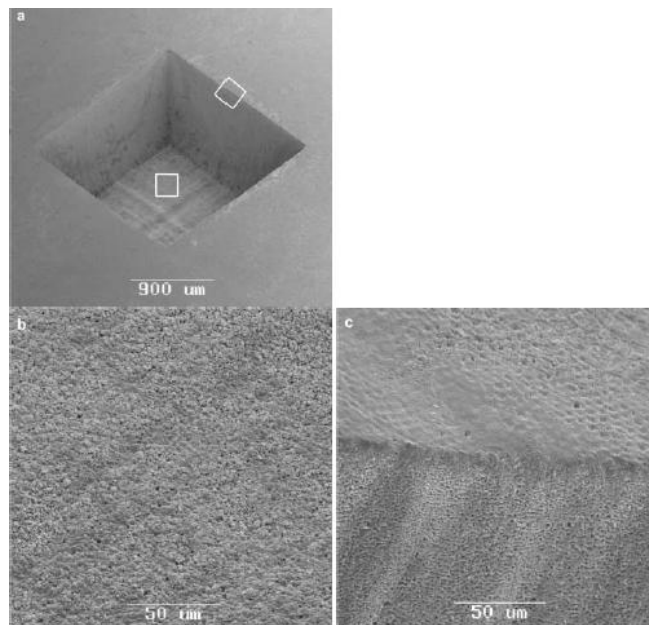


Fig. 3.3. SEM of a cavity 2mm \times 2mm \times 1.4mm (a), its bottom (b), and one of its side walls (c) (target: healthy dentin, processed by $\lambda = 780$ nm, $t = 700$ fs, $E = 100$ μJ , repetition rate is 5 kHz)

Even here, excellent quality is achieved as demonstrated in the enlargement (Fig. 3.5b). Carious enamel is removed without breaking apart. Small microcracking proved to be superficial only, indicating that this artefact was caused by the drying process during the SEM preparation. When comparing femtosecond laser dentistry with previous dental laser applications, the quality achievable with femtosecond laser pulses is impressive. This quality is primarily

due to the single fact that femtosecond laser interaction with biological tissues is a direct multiphoton ionization of bound and free electrons, which leads to pure plasma-induced ablation [6] of the material. Focusing of femtosecond laser pulses to spot sizes of several micrometers leads to so high intensities that these free electrons are generated at pulse energies in the range of a few microjoules and in a very thin layer of material of less than 1 μm , resulting in a well-defined optical breakdown, called “ablation threshold” , which is independent of the beam size and repetition rate for a fixed pulse duration [4].

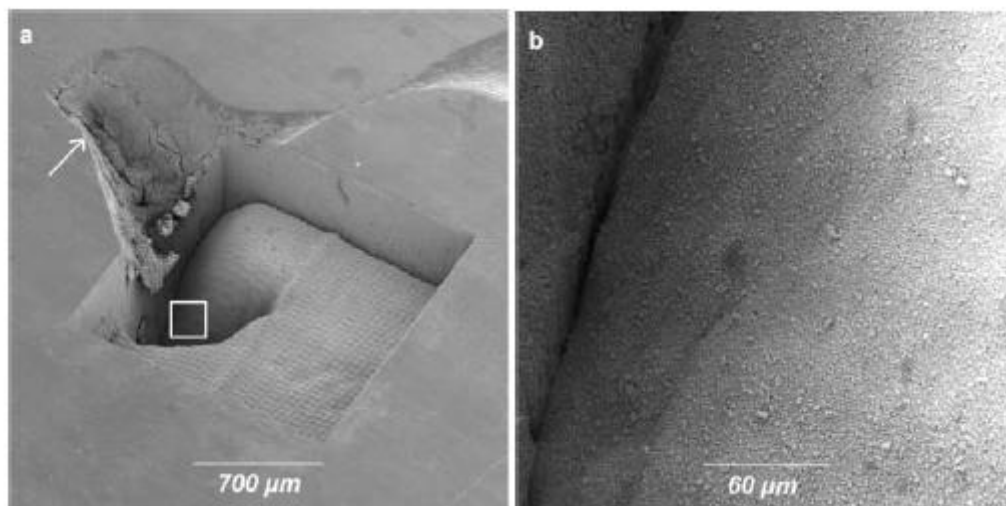


Fig. 3.4. (a): SEM of a cavity with a carious lesion (white arrow) and its bottom (target: healthy dentin with a carious lesion at the tip of the white arrow). (b): Enlargement of (a) shows a caries-free surface

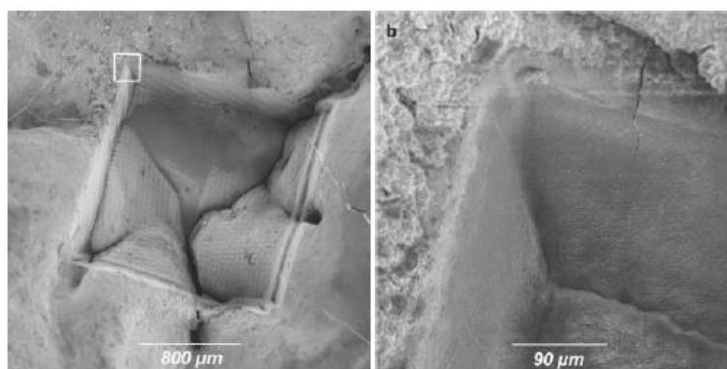


Fig. 3.5. (a) SEM of a cavity (target: carious enamel at an occlusal fissure). (b) Enlargement of (a) shows a caries-free surface at the corner of the cavity

This ultrafast and minimally invasive laser-tissue interaction shows why the use of femtosecond laser pulses for tooth hard tissue ablation minimizes mechanical and thermal effects. It proves that precise structuring is possible without collateral injuries and most probably without activation of damage-sensing neurons, called nociceptors. Therefore, the excavation of caries is expected to be at least significantly pain reduced, maybe completely pain free. As a result, the femtosecond laser ablation is significantly superior to laser material processing

with pulses longer than 1 ps and to the conventional tooth preparation by mechanical drills.

§3.2. Ophthalmic Applications

Femtosecond photodisruption opens new pathways in refractive surgery due to its precise interaction mechanism with biological tissue. The quality of tissue processing allows correction of refractive errors and preparing donor and recipient tissue for keratoplasty with a much higher flexibility of what is known from the use of mechanical knives. In this chapter, the potential of ultrashort laser pulses is shown in the field of refractive surgery, keratoplasty and the treatment of presbyopia.

One way to overcome the problems of creating a flap with a microkeratome is by using ultrashort laser pulses. The principle of this procedure is shown in Fig. 3.6. In the first step, a lamellar intrastromal cut is performed by scanning the laser in a spiral pattern. This procedure is analogous to the mechanical lamellar cut of a microkeratome (diamond knife) in the conventional LASIK procedure. But not only can the troublesome lamellar LASIK cut be done with the femtosecond laser. In a second step, another cut prepares a stromal lenticule with the desired shape, depending on the refractive error of the treated eye. In the third step, the anterior corneal flap is opened, and the prepared lenticule can be extracted [7, 8, 9]. Finally, the flap will be repositioned on the cornea. The surface of the cornea follows the missing volume of the lenticule, thereby leading to a change in refractive power. Although the mechanical and thermal damage of the surrounding tissue were already shown to be small, several other side effects may take place, due to the nonlinear character of the photodisruption.

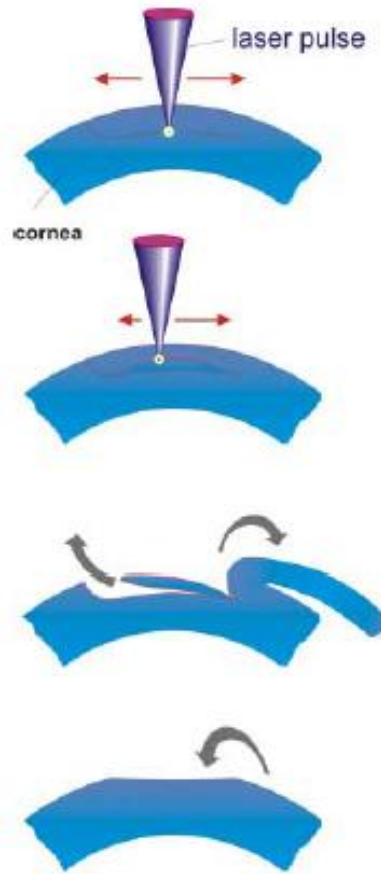


Fig. 3.6. Principle of femtosecond laser keratomileusis

§3.3. Neurosurgical Applications

The high precision of femtosecond laser ablation makes it an interesting tool for neurosurgical applications. The resection of arbitrary-shaped volumes of brain tissue can be of interest for the treatment of movement disorders. Fundamental studies of bovine brain-tissue ablation have shown precise cutting effects of femtosecond laser pulses with no thermal or structural side effects. If a large number of laser pulses is applied with an appropriate strategy, the quality of the laser cut is comparable to a mechanical cut with a scalpel. A selection of important requirements for the application of these laser pulses with a neurosurgical instrument are presented with respect to navigation, beam delivery, and operation monitoring [10, 11].

Ablation of bovine brain has shown precise cutting effects without thermal or structural changes to adjacent tissue. In addition, the ablation with femtosecond laser pulses was found to be more efficient than the ablation with picosecond laser pulses: Laser pulses from a Ti:sapphire laser with 140 fs duration showed a two times higher efficiency than the longer 30 ps from a Nd:YLF laser with identical pulse energy. The same fundamental study has shown that the threshold fluence needed for initiating the ablation process is lower for the shorter femtosecond laser pulses than for picosecond or nanosecond laser pulses [12]. The ablation threshold

of bovine tissue was at 1.5 J/cm^2 for 100 fs and at 20 J/cm^2 at pulse widths of 35 ps. Therefore, lower pulse energies can be used for the removal of neural tissue if femtosecond laser pulses are applied. As discussed with reference to ophthalmic applications, the decrease of the applied pulse energy leads to smaller sizes of cavitation bubbles as well as less extensive shock-wave formation. In contrast to the transparent cornea the brain tissue absorbs infrared laser radiation to a high extent and the ablation takes place on the tissue surface. However, since the laser pulses are applied through a minimally invasive instrument, ablation within a rinsing liquid has to be considered. Therefore, the reduction of cavitation bubbles is important.

§3.4. Subcellular Photodisruption

Laser micromanipulation can be used in various applications at the cellular level. For example, single organelles, cytoskeletal filaments, chromosomes, flagella, mitochondria can be cut or altered in their functionality. Moreover, it is possible to perforate cell membranes by a laser beam, in order to induce cell fusion or enable the transfer of foreign DNA into the cell, so-called optoporation or, in the case of a single cell, optoinjection.

Near-infrared laser radiation has a very high penetration depth in biological samples, due to the so-called optical window. If ultrashort laser pulses (100 fs to 200 fs) with wavelengths in the near infrared are focused very tightly by microscope objectives (0.9 NA or higher), precision at the cellular level can be achieved by nonlinear absorption. This absorption is very well confined to the focus region, due to the intensity dependence of the nonlinear effects. The applied pulse energies are in the range of only 0.5 nJ to 4 nJ. However, the first application of femtosecond pulses in the field of singlecell manipulation was for illumination purposes in multiphoton microscopy. To achieve a higher resolution during the excitation of a sample and to reduce out of focus photobleaching or damage, a tightly focused ultrashort laser beam is used to induce the excitation by simultaneous absorption of photons. Thereby, only in a small volume at the focus region are the intensities high enough to reach the threshold for multiphoton processes. The axial resolution is several times higher when compared to conventional illumination and comparable to a conventional confocal laser scanning microscope [13, 2].

Cell surgery was first performed by König et al., by raising the pulse energy of the multiphoton illumination source up to the nanojoule level. As can be seen in the atomic force microscopy image in Fig. 3.7, the processing of single chromosomes becomes possible, offering resolutions of about 100 nm. The image shows several cuts through human chromosomes, having a minimum cutting size of 110 nm. In the lower part several chromosomes with a hole drilled into them with diameters in the 100 nm range are shown. The minimum volume of ablated material was approximately $0.008 \text{ } \mu\text{m}^3$ at an exposure time of 1.3 ms, which represents roughly 10 000 laser pulses. At similar pulse durations but at kHz

repetition rates the group of Eric Mazur showed the application of ultrashort laser pulses to dissect single mitochondria in living cells (Fig. 3.8). The picture was taken by a fluorescence microscope, through which the ultrashort laser beam was focused onto the targeted cell. The epithelial cell remained alive after the processing by the laser.

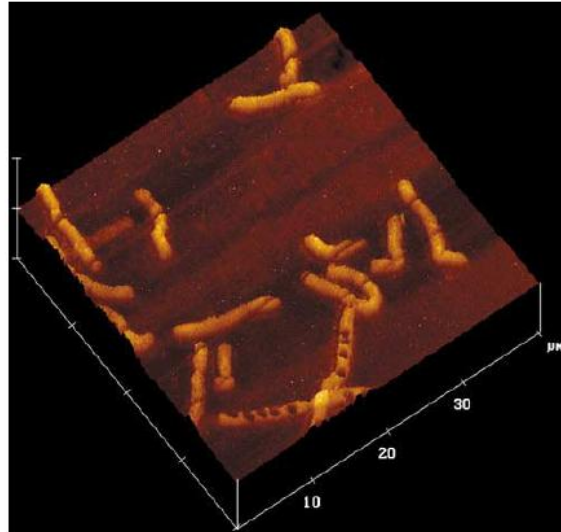


Fig. 3.7. Human chromosomes treated by 100 fs laser pulses at 800 nm, the linear cuts have a minimum diameter of 110 nm, the holes have diameters in the range of some hundred nanometers

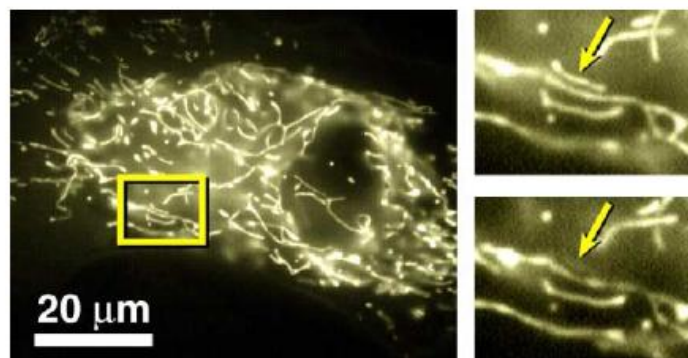


Fig. 3.8. Cut in a capillary endothelial cell by a 2 nJ pulse at a pulse duration of 100 fs at 800 nm. The mitochondrion in the square is cut by 1 s illumination by the ultrashort laser, see detail on the right. After treatment the cell remains alive

REFERENCES

- [1] Dausinger F., Lichtner F., Lubatschowski H. Femtosecond Technology for Technical and Medical Applications. © Springer-Verlag Berlin Heidelberg, P. 321, 2004.
- [2] Shi, L. and Alfano, R.R. eds. Deep imaging in tissue and biomedical materials: using linear and nonlinear optical methods. © CRC Press. 2017.
- [3] Dausinger F., Lichtner F., Lubatschowski H. (Eds.): Femtosecond Technology for Technical and Medical Applications, Topics Appl. Phys. **96**, 91–105, 2004.

- [4] Vogel A., Venugopalan V.: Mechanisms of pulsed laser ablation of biological tissues, *Chem. Rev.* 103, 577–644, 170, 2003.
- [5] de Menezes, Rebeca Ferraz, Catherine Malinda Harvey, Marleny Elizabeth Márquez de Martínez Gerbi, Zachary J. Smith, Dan Smith, Juan C. Ivaldi, Alton Phillips, James W. Chan, and Sebastian Wachsmann- Hogiu. "Fs- laser ablation of teeth is temperature limited and provides information about the ablated components." *Journal of Biophotonics*, V. 10(10), pp.1292-1304, 2017.
- [6] Kim B. M., Feit M.D., Rubenchik A.M., Joslin E. J., Celliers P.M., Eichler J., Silva L.B. D.: Influence of pulse duration on ultrashort laser pulse ablation of biological tissues, *J. Biomed. Opt.* 6, 332–338, 171, 2001.
- [7] Lubatschowski H., Maatz G., Heisterkamp A., Hetzel U., Drommer W., Welling H., Ertmer W.: Application of ultrashort laser pulses for intrastromal refractive surgery, *Graefes Arch. Clin. Exp. Ophthalmol.* 238, 2000.
- [8] Heisterkamp A., Thanongsak M., Kermani O., Drommer W., Welling H., Ertmer W., Lubatschowski H.: Intrastromal refractive surgery with ultrashort laser pulses – in vivo study on rabbit eyes, *Graefes Arch. Clin. Exp. Ophthalmol.* 241, 511–517, 2003.
- [9] Wang, Y., Du, J., Yang, M., Xu, Y., Guan, H. and Wu, J. Distinct macular thickness changes after femtosecond laser–assisted cataract surgery of age-related cataract and myopia with cataract, *Scientific reports*, 8(1), p.3279, 2018.
- [10] Santos, S.I., Mathew, M. and Loza-Alvarez, P. Real time imaging of femtosecond laser induced nano-neurosurgery dynamics in *C. elegans*, *Optics express*, 18(1), pp.364-377, 2010.
- [11] Losel F.H., Fischer J. P., G€otz M.H., Horvath C., Juhasz T., Noack F., Suhm N., Bille J. F.: Non-thermal ablation of neural tissue with femtosecond pulses, *Appl. Phys. Lett.* 66, 121–128, 1998.
- [12] Losel F.H., Niemz M.H., Bille J. F., Juhasz T.: Laser-induced optical breakdown on hard and soft tissues and its dependence on the pulse duration: Experiment and model, *IEEE J. Quantum Elect.* 32, 1996.
- [13] Konig K.: Laser tweezers and multiphoton microscopes in life sciences, *Histochem. Cell. Biol.* 114, 79–92. 2000.

Chapter 4. THz optics and spectroscopy

§4.1. Methods of generating terahertz pulses with femtosecond lasers

§4.1.1. Introduction

Creation of an efficient, powerful, inexpensive, and compact source of superbroadband terahertz THz pulses that operates at room temperature is one of the main challenges in modern photonics [1]. The superbroadband THz radiation offers enormous potential for a wide range of technical and scientific applications: the diagnosis of various materials, including semiconductors, chemical compounds, biomolecules, and biological tissues; the formation of images, tomography, and endoscopy for medical purposes and safety; remote control and monitoring of the environment; astronomy; etc. [2,3]. The THz range actually covers a wide region of vibrational, rotational, and translational lines of a broad class of organic and biological molecules. The unobstructed penetration through fog and haze, rain, paper, wood, plastic, ceramic, and other materials because of the smallness of the Rayleigh scattering of radiation in this region opens up wide possibilities for endoscopy with resolution all the way to 100 μm and high SNR. The low energy of the THz quanta and the associated nonionizing character of the action of the THz radiation opens up wide possibilities for using it in biology and medicine. At the same time, the energy of THz quanta corresponds to the vibrational energy of important biological molecules, including DNA and RNA, and thus makes it possible to accomplish purposeful action on them both for research and for medical purposes, stimulating or suppressing the development of viruses, cells, and their components. No less promising from a practical viewpoint is the use of THz radiation in medicine for the visualization, holography [4], and tomography of tissues, therapy, and surgery.

In the last twenty years, along with the development of femtosecond solid-state lasers especially lasers based on sapphire crystals doped with titanium ions and microelectronics, a significant shift has been noted in studies of the THz region. Three methods of obtaining ultrashort THz pulses have been most actively developed, using femtosecond laser sources: generation by photoconductive antennas, nonlinear-optical generation of the difference frequency or optical rectification, and generation with the use of optical breakdown in gases under the action of femtosecond pulses. These methods make it possible to obtain THz electromagnetic radiation with peak electric-field amplitudes up to 1MV/cm by using femtosecond laser systems with amplifiers [5].

§4.1.2. THz generation by photoconductive antennae I

One of the first methods for generating THz radiation was by implementing a photoconductive antenna by irradiation with picosecond pulses [6]. A photo-

conductive antenna comprises a fast optically activated switch which is embedded in an antenna structure. In practice, this usually takes the form of metal electrodes on a semiconductor substrate, with a geometry similar to that shown in Fig. 4.1.

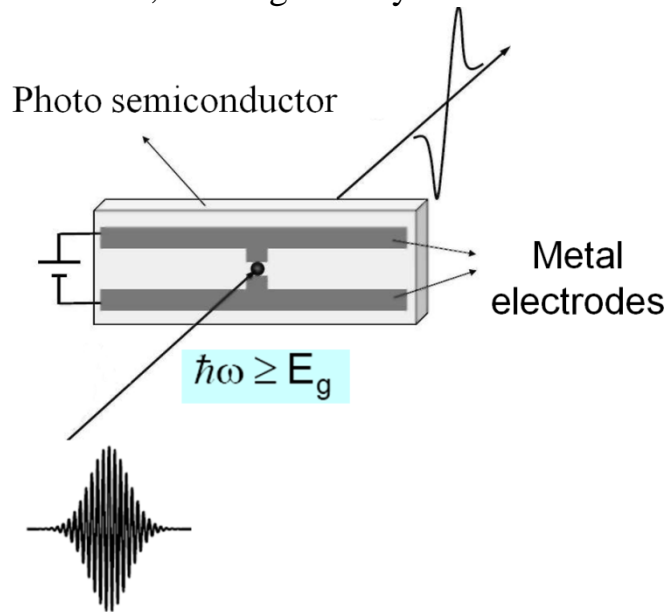


Fig.4.1. Photo-conductive antenna, the femtosecond pulse arrives from the *left* and the THz field is radiated to the *right*.

The femtosecond optical pulse is focused into the gap between two electrodes. The effect by which electromagnetic radiation is generated by the surface of a semiconductor, that is, a photoconductive antenna, when it is excited by ultrashort femtosecond pulses, is explained by the dynamics of the formation of photocarriers—electron-hole pairs—and their superfast motion in a near-surface electric field. According to Maxwell's equations, the current $J(t)$ that appears in this case causes an electromagnetic pulse $E(t) \sim dJ(t)/dt$ to be generated, usually in the form of one cycle, with a spectrum determined by the Fourier transform of its temporal shape. The surface of the semiconductor thus operates as a dynamic photoconductive antenna that emits pulses of broadband electromagnetic radiation with a width of hundreds of femtoseconds. The central frequency of the radiation generated by the photoconductors is usually in the 1–2-THz region. Semiconductor crystals of GaAs, InP, and InAs are widely used as generators of THz radiation [1, 2]. To increase the efficiency of the THz emission, the crystal samples are placed in strong electric or magnetic fields [7]. It should be pointed out that, according to the model of Ref. 8, the intensity of the THz radiation is proportional to the time derivative of the concentration of electron-hole pairs and their speed in an electric or magnetic field, which is determined by the mobility of the charge carriers. One of the highest electron mobilities—about $3 \cdot 10^4 \text{ cm}^2/\text{V sec}$ —is possessed by undoped InAs crystals, and these crystals currently exhibit the highest conversion efficiency of femtosecond laser radiation into THz pulsed radiation [8].

Up to now we have only discussed the use of photo-conductive antenna for the generation of THz radiation, the same devices can be used for detection of THz

radiation. When used for detection a femtosecond ‘probe’ pulse is focused onto the device Fig.4.1, generating electron–hole pairs, as above. The incident electric field of THz pulse, E_{THz} , then accelerates these charges before they are again recaptured. The current produced is amplified and converted to a voltage, and then usually detected using sensitive lockin techniques. The voltage is proportional the incident electric field of THz pulse, E_{THz} .

§4.1.3. THz generation by optical rectification I

The large peak value of the electric field of the radiation of a femtosecond pulse in the visible or near-IR regions makes it possible to use the second-order nonlinear susceptibility $\chi^{(2)}$ of electrooptic crystals to generate THz radiation. The nonlinear interaction between any two frequency components within the spectrum of a femtosecond pulse causes polarization $P(\omega_{\text{THz}})$ of the medium, as a result of which the electromagnetic waves are emitted at the beat frequency, with the polarization of the medium being proportional to the incident pulse intensity; i.e, it is possible to write:

$$P(\omega_{\text{THz}}) \sim \chi^{(2)}E(\omega_1)E(\omega_2) \sim \chi^{(2)}E_0^2 \quad (4.1)$$

in the frequency region, where $E(\omega_1)$ and $E(\omega_2)$ are the Fourier components of the spectrum of the femtosecond pulse, while $\omega_{\text{THz}} = \omega_1 - \omega_2$. In the dipole approximation and in the far zone of diffraction, the amplitude of the THz wave is proportional to the second derivative with respect to time of the optically induced polarization, $E(\omega_{\text{THz}}) \sim d^2P/dt^2$. Since the width of the spectrum the pulse width of femtosecond radiation is usually 10 THz (100 fs), the upper limit of the spectral width and the lower limit of the pulse width of THz radiation must be about the same.

Optical rectification has been used for the generation of THz radiation in many electrooptic crystals, such as ZnSe, GaSe, and ZnTe [9] as well as in the organic ionic salt N-4- dimethylamino-4-N-methylstilbazolium tosylate DAST [10]. Besides the value of the second-order susceptibility, the conversion efficiency into THz radiation depends on the relationship of the phases of the interacting waves; i.e., the following phase-synchronization condition should be satisfied:

$$\Delta k = k_1 - k_2 - k_{\text{THz}} = 0, \quad (4.2)$$

where Δk is the wave detuning between the wave vectors k_1 and k_2 of the pump waves and the wave vector k_{THz} of the THz pulse. In many nonlinear optical materials, such as LiNbO₃, phase matching between the THz wave and the pump wave cannot be achieved, because the refractive index of the given materials at THz frequencies is significantly greater than that in the visible and near-IR regions. It has been shown [11] that the length of coherent interaction (the coherence length l_{coh}) depends largely on the mismatch of the group velocity of the femtosecond pump pulse and the phase velocity of the THz pulse and is determined by

$$L_{\text{coh}} = \frac{\pi c}{\omega_{\text{THz}}(n_{\text{gr}} - n_{\text{THz}})}, \quad (4.3)$$

where $n_{\text{gr}}(\lambda) = n(\lambda) - \lambda(dn/d\lambda)_\lambda$ is the refractive index of the crystal for the group velocities of the femtosecond pulse, n_{THz} is the refractive index of the medium at the THz frequency, and c is the speed of light. Phase matching is observed in such nonlinear materials as ZnTe, GaSe, and DAST, in which l_{coh} is 0.1–1 mm. It should be pointed out that the organic crystal DAST has the greatest nonlinear susceptibility $d_{111} = 1010 \text{ pm/V}$ among these nonlinear media at a wavelength of 1318 nm [11]. Many groups of researchers use ZnTe crystals, which have a nonlinear susceptibility of $d_{14} = 4 \text{ pm/V}$ at the titanium-sapphire-laser wavelength of $\lambda = 800 \text{ nm}$, with the coherence length making it possible to generate electromagnetic vibrations in the range from 0 to 2 THz.

As mentioned above, for efficient nonlinear generation of THz, phase matching between the optical and THz pulses is required. One novel method for achieving this is by tilting the EO crystal, in particular this has been done successfully with LiNbO₃ [12]. Lithium niobate is a widely used EO crystal because it is highly transparent and has a large EO coefficient (the largest is $d_{33} = 27 \text{ pm/V}$), however, because of the refractive index mismatch it is not efficient for generating THz in the collinear geometry described above. This mismatch can be overcome by titling the optical pulses, shown in Fig. 4.2, so that the pulse front of the optical pulse travels at the THz phase velocity.

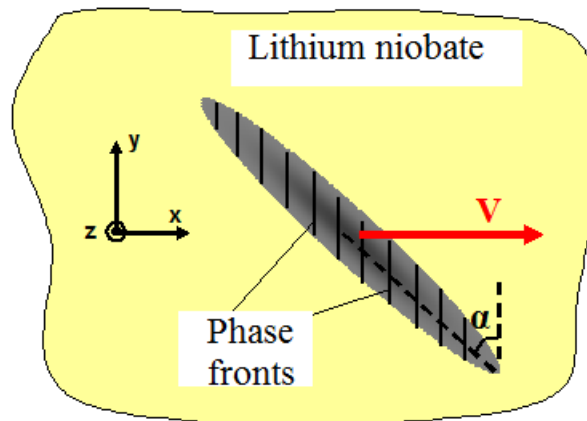


Fig.4.2. Generation of THz pulses in LiNbO₃. The femtosecond pulse is tilted by a grating, as it propagates through the nonlinear medium it remains in phase with the generated THz pulses.

§4.1.4. THz generation using optical breakdown I

The generation of THz radiation in which the fundamental and the second harmonic of a femtosecond laser are focused in air is one of the newest methods of generating THz radiation and does not require the presence of any special medium

[13-16]. There are several explanations of the generation mechanism. Thus, Cook and Hochstrasser [13] connect the appearance of radiation of the difference frequency with four wave mixing of the radiation of the first and second harmonics of a femtosecond pump laser at third-order plasma nonlinearity $\chi^{(3)}$. The process is described as follows: polarization $P(\omega_{\text{THz}})$ at a THz frequency arises when three waves interact—two pump waves at the fundamental frequency, $E(\omega_1)$ and $E(\omega_2)$, and a wave of the second harmonic, $E(2\omega)$; i.e.,

$$P(\omega_{\text{THz}}) \sim \chi_{i,j,k,l}^{(3)} E(2\omega) E(\omega_1) E(\omega_2). \quad (4.4)$$

It should be pointed out that, for THz radiation to appear, the presence of a plasma (optical breakdown of the gas) — the appearance of free electrons — is necessary in this case. Another explanation of the effect is based on the transverse plasma-current model, resulting from the liberation of electrons from the gas molecules as a consequence of tunnel ionization. The resulting electrons are accelerated in the asymmetric laser field formed by adding the vibrations of the first and second harmonics [14, 15], and this results in the appearance of a nonzero projection of the velocity in the transverse direction — transverse current. Since the process is strongly nonsteady-state and occurs at the instant that the laser pulse acts ($\tau \leq 100$ fs), current $J(t)$ causes the generation of an electromagnetic pulse $E(t) \sim dJ/dt$, thus generating an electromagnetic pulse at THz frequencies.

As a consequence of the given method, THz pulses were obtained with an energy of several microjoules, a lasing band width of 200 THz, and an electric field around 1MV / cm at a frequency of 2 THz [16].

§4.1.5. Experimental apparatus

The generalized layout of the apparatus for generating THz radiation using various methods is shown in Fig. 4.3a. The beam diameter of the THz radiation with central wavelength λ at distance L from the radiating surface of the generator can be estimated from $D(L) = L \sin\theta$, where $\theta = 1.22\lambda/2r_0$ is the diffraction divergence of a beam of radius r_0 , which is determined by the size of the excited region. Computations show that, for $\lambda = 300 \mu\text{m}$ (1 THz) and $2r_0=500 \mu\text{m}$ at a distance of 120 mm from the THz-radiation generator, the beam has a diameter of 80 mm. Therefore, to carry out experiments with this radiation, we used parabolic mirrors with a principal focus of 120 mm and an aperture of 90 mm. A filter made from black Teflon eliminated the pump radiation incident on the optoacoustic detector (OAD) – Golay cell. The mean power of the generated THz radiation was measured by a nonselective OAD with internal filters that transmitted electromagnetic radiation in the range 50–600 μm . The OAD was a sealed chamber filled with xenon, in which a spectrally nonselective radiation absorber and an optical microphone were placed. The electric signal from the optical microphone arrived at an amplifier with a gain of up to 10^4 and then at a synchronous detector coupled with the modulator of the input optical radiation.

The minimum power that could be recorded by the detector system described above was about 1 nW.

To create a magnetic field parallel to the surface of the semiconductor crystal, which is most effective for generating THz radiation, the sample was placed in a specially developed magnetic system based on a Nd:B:Fe composite with a magnetic field of 1.8...2.3 kOe at the point of excitation of THz radiation (Fig. 4.3b). The magnetic system is a vertical cylinder 100 mm in diameter and 140 mm high, with two horizontal wedge-shaped recesses that communicate at the center of the magnetic system, 10.5 mm high. The semiconductor crystal was placed at the center of the cylinder on its axis, so that the pump radiation was incident on it through one aperture, while the reflected and THz radiation escaped through another.

As generators of THz radiation we used an undoped InAs semiconductor crystal located in the magnetic field, a ZnTe electrooptic crystal, a DAST organic crystal (Fig. 4.3c), and an optical spark in air.

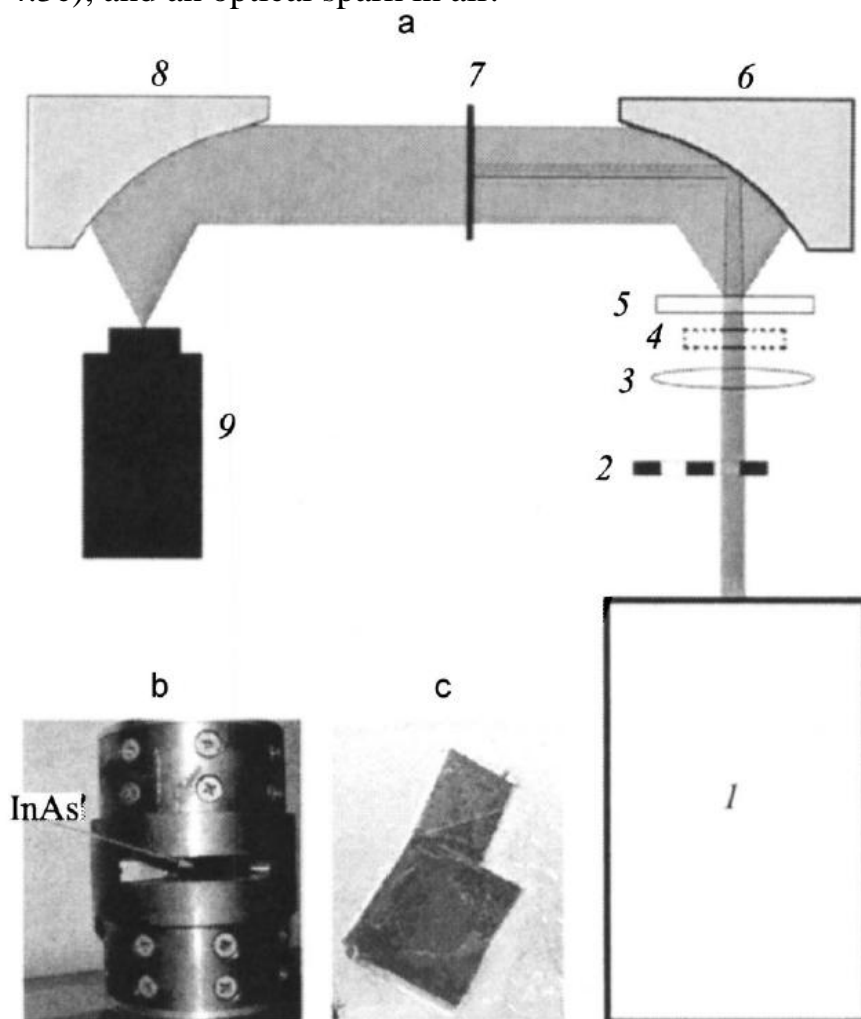


Fig. 4.3. (a) Optical layout for measuring the mean power of THz radiation. 1 — femtosecond laser, 2 — modulator, 3 — lens, 4 — BBO crystal, 5 — generator of THz radiation, 6 and 8 — parabolic mirrors, 7 — filter, 9 — OAD. (b) Magnetic system; (c) N-4-dimethylamino-4-Nmethylstilbazolium tosylate (DAST) crystal.

§4.1.6. THz generation by photoconductive antennae II

An undoped InAs crystal, cut on the [100] plane and consisting of a 5x5-mm plate 300 μm thick, was used as a THz generator. The concentration of most carriers in the crystal was of about $3 \cdot 10^{16} \text{ cm}^{-3}$ and the electron mobility was of $3 \cdot 10^4 \text{ cm}^2 / \text{V sec}$.

To increase the energy density, the radiation of femtosecond laser (FLS) with $f=100 \text{ cm}$ lens was focused on the surface of the crystal in a spot of 500 μm in diameter, with the plane of the InAs crystal at an angle of 45° to the incident beam, since, as a consequence of the high refractive index for the far-IR region, THz radiation experiences total internal reflection, and the reflected radiation can be totally directed to a parabolic mirror.

When pulses of the FLS with a single-pulse energy up to 1 nJ and a mean power of 50 mW were focused on the InAs surface with no magnetic field, THz radiation with mean power 2 nW was recorded. Placing the InAs in a 1.8-kOe magnetic field in a direction parallel to the crystal surface increased the power of the generated radiation to 150 nW. The dependence of the mean power of the THz radiation on the mean pump power was quadratic, and this agrees with the experimental data of Ref. 7 and the theory of Ref. 17 for optical-excitation energy densities below the saturation density. The maximum conversion efficiency η , defined as the ratio of the emitted mean power W_{THz} of the THz radiation to the mean power W_0 of the optical radiation incident on the crystal, was obtained at a value of $W_0 = 100 \text{ mW}$ and equalled $\eta \approx 10^{-6}$.

When pulses of the FLS with a single-pulse energy of up to 1 mJ and a mean power of up to 50 mW were focused on the surface of the InAs in the magnetic system, the maximum conversion efficiency increased to $\eta \approx 10^{-5}$. When the dependence of the mean power of the THz radiation on the mean power was studied, saturation was clearly observed when the power density of the radiation was 10^{-4} J /cm^2 or with a radiation flux of $10^{14} \text{ photon/cm}^2$, approximately corresponding to the number of majority carriers in the near surface layer of the crystal.

§4.1.7. THz generation by optical rectification II

When pulses of the FLS with single-pulse energy up to 1 mJ and mean power up to 50 mW were focused and after they passed through a ZnTe crystal 4 mm thick or a DAST crystal 100 μm thick, a spectral supercontinuum was generated [18]; therefore, a starting laser beam 5 mm in diameter was used in the experiments. Under these conditions, a mean THz-radiation power reaching 100 nW was obtained in the ZnTe crystal. When the DAST crystal was used in the same geometry and with the same pump parameters, the mean THz-radiation power increased and reached 800 nW.

As is well known [10, 11], DAST is a uniaxial nonlinear-optical crystal; the generation efficiency of the THz radiation accordingly depends on the relative alignment of the DAST crystal's crystallographic axes and the polarization of the radiation. Figure 4.4 shows how the THz-radiation intensity depends on the crystal's angle of rotation. The pronounced maxima show that the generation efficiency depends on the relative alignment of the crystal's axes and the polarization of the exciting radiation. The 0° – 180° direction (Fig. 4.4) corresponds to the vertical axis of the DAST crystal in Fig. 4.3c, with the polarization of the pump radiation being horizontal.

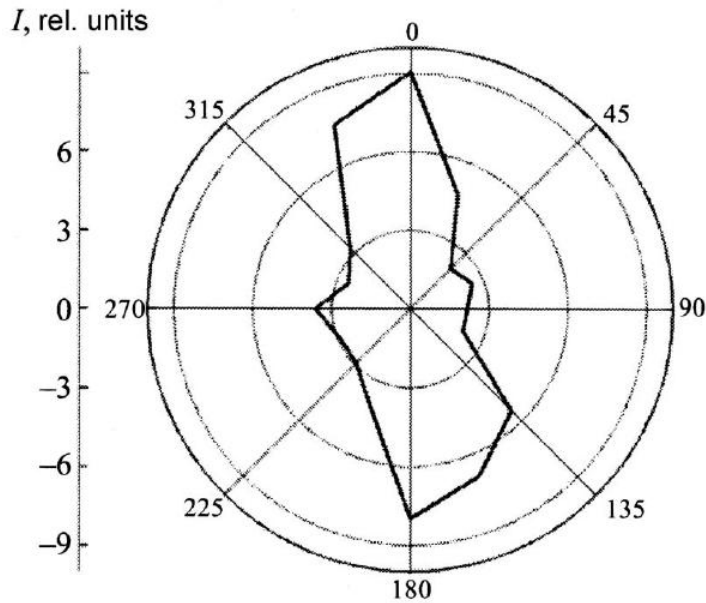


Fig. 4.4. Dependence of the generation intensity I of THz radiation on the rotation angle of the DAST crystal.

The high conversion efficiency in the DAST crystal made it possible to measure the beam's spatial profile by the Foucault knife-edge method (Fig. 4.5). Knowing the beam profile between the parabolas and the size of the excited region of the crystal, it is easy to calculate the frequencies that contribute the most to the emission spectrum. Starting from the diffraction calculations, it was shown that the maximum of the THz emission spectrum comes at about a frequency of 1.2 THz.

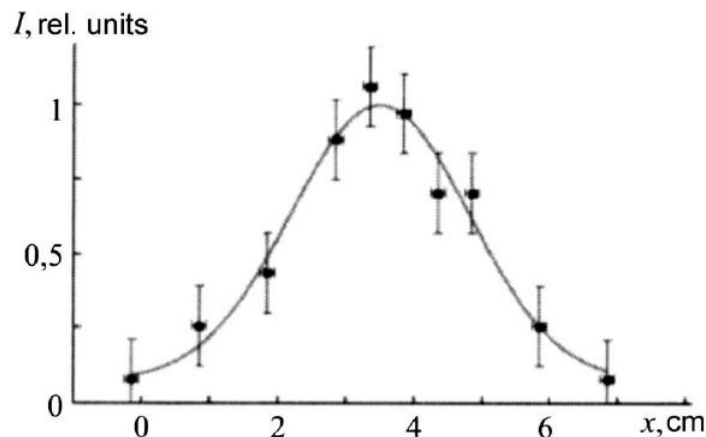


Fig. 4.5. Profile of THz beam accompanying excitation in the DAST crystal.

§4.1.8. THz generation using optical breakdown II

The experiments were carried out using the layout shown in Fig. 4.3, with a β -BBO crystal that generates second harmonic radiation ($\lambda = 400$ nm), placed between the lens and its focus in order to make the pulses of the first and second harmonic coincide in time. The crystal was attached to a linear translator and was displaced along the beam axis to provide accurate phase locking between the waves of the first and second harmonics. Calculations show that, when two-color radiation passes through a lens 10 mm thick, as a consequence of the dispersion of the glass and, accordingly, the different group velocities of the two pulses, the pulse of the first harmonic outruns the pulse of the second by 50 fs. When it propagates in air, the dispersion between the pulses of the first and second harmonics is 0.257 fs/cm.

An FLS was used in the experiments, and the optical breakdown threshold in air was at a total single-pulse energy of the first and second harmonic of about 100 μ J (the mean power is 5 mW). Radiation of the THz range and a spectral supercontinuum appeared at the same time as the breakdown. As the BBO crystal moved along the beam axis in the direction of the focus of a lens having $f = 15$ cm, a sinusoidal variation of the mean THz-radiation power with contrast above 50% was observed. With the maximum total single-pulse energy of the first and second harmonic of $W \approx 1$ mJ and a mean power of 50 mW, a mean THz power of up to 20 nW was obtained, with the dependence of the mean THz power on the mean pump power being close to exponential. The sinusoidal variation of the mean THz-radiation power when the BBO crystal moves along the beam axis can be explained by the addition of the electric fields of the waves of the first and second harmonics of the radiation of the FLS and by the motion of the plasma electrons in the given biharmonic field. This is shown by the fact that a period of variation equal to 30 mm corresponds to a delay time of 0.77 fs between pulses of the first and second harmonics of the FLS radiation because of the dispersion of air and approximately corresponds to half the vibrational period at a wavelength of $\lambda = 400$ nm ($T = 1.33$ fs) and a quarter of the vibrational period at a wavelength of $\lambda = 800$ nm ($T = 2.67$ fs).

§4.2. Time-resolved THz spectroscopy

There are currently numerous papers associated with ultrashort THz pulses and devoted to questions of spectroscopy, including time-resolved spectroscopy [3, 19-21]. THz spectroscopy makes it possible to measure spectra in the frequency range 0.2–2 THz or 6.6–66 cm^{-1} , and this is very important for studies of organic molecules that contain hydrogen and carbon bonds.

In a THz time-domain or pulsed system, a laser pulse is split in two beams. One of the beams is referred as the pump beam and the other one is referred as the probe beam. The pump and probe pulses are derived from the same optical beam

and, therefore, have the same pulse duration, which typical has a range between 20 to 120 fs. The energy of the pump beam is much larger than the energy of the probe beam because the pump beam is used to generate the THz pulse. In the most basic configuration, the pump beam generates an electromagnetic transient, through the excitation of a semiconductor or electro-optical material. This electromagnetic transient is the THz pulse. The duration of the THz pulse is in the range of few ps, which is larger than that of the pump beam. The probe beam is used to detect the THz pulse through the inverse process for the THz generation. The detection of the THz pulse provides the waveform, which is the amplitude of the electric field of the THz pulse as a function of the timing difference between the probe and pump beams. The timing difference between the pump and probe beams is controlled so the response of the sample to the pump beam as a function of time can be measured very precisely. The most common way to control the timing difference is by using a mechanical delay line in the pump beam. A time delay changes the path length path of the beam and, thus, changes the relative timing between the pump and probe pulses. Other methods to control the time difference include changing the refractive index of a section of the optical path of one of the beams by using materials such as liquid crystals. However, such material offer a limited time delay range and are slow to respond. The maximum difference between the pump and probe is referred to the delay range. Delay ranges for common THz time-domain systems go from 10 ps to 100 ps. However, delay ranges up to 1 ns or more are necessary for certain standoff and high resolution spectroscopy applications.

The standard system of a THz spectrometer with time resolution is shown in Fig. 6. Laser beam from a femtosecond *Yb:KYW* laser *FL-1* (wavelength $\lambda_p = 1040$ nm, beam diameter $d = 2$ mm, the pulse width at half-width $\tau \approx 200$ fs, repetition rate of 80 MHz, average power $W = 1.2$ W) with use of a beam splitter *BS* is divided into a probe beam and a pump beam. The pump beam passes through an optical delay line (Delay). It falls on a semiconductor crystal *InAs*, placed in a constant magnetic field *M*, where THz radiation is generated. Plane of the crystal coincides with the focal plane of a parabolic mirror *PM1* with focal length of 90 mm and an optical aperture of 60 mm. THz radiation is collimated by a parabolic mirror *PM1* behind which there is a teflon filter *F*, transmitting terahertz radiation and scattering powerful infra-red radiation. In addition horizontal polarization is emphasized by a polarizer *P*. After passage of the optical path in the air $L = 25$ cm.

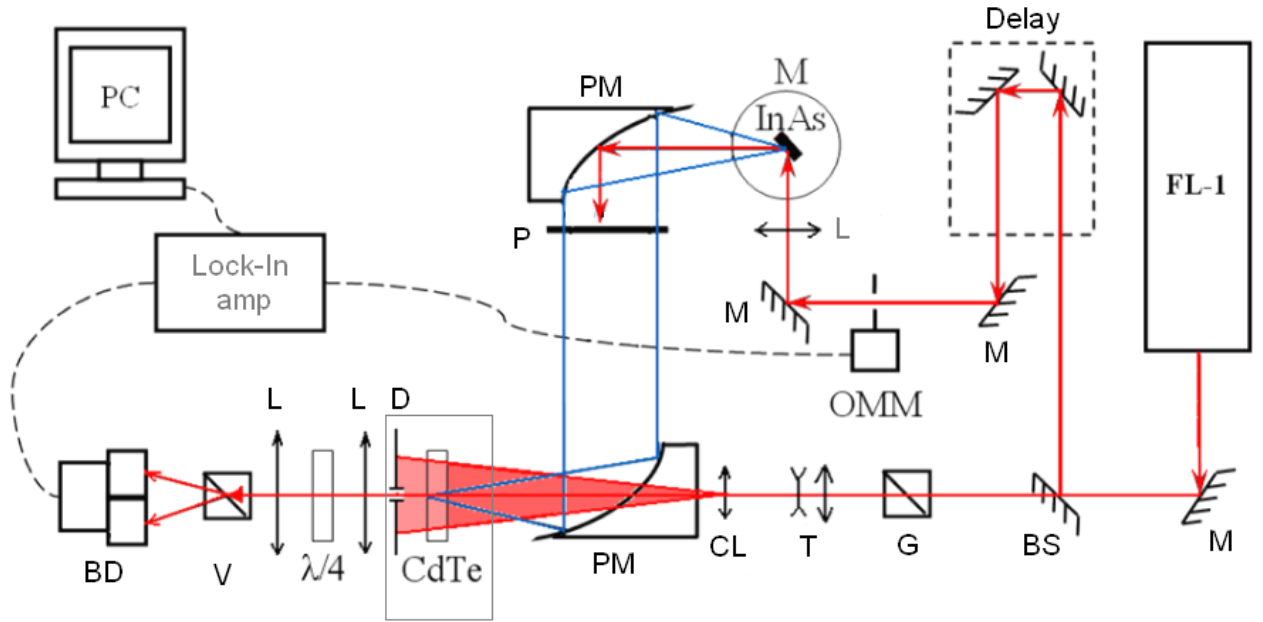


Fig. 4.6. The experimental scheme: *Yb: KYW laser FL-1* ($\lambda = 1040 \text{ nm}$, $\tau \approx 200 \text{ fs}$, repetition rate of 80 MHz, $W = 1.2 \text{ W}$); *BS*-beam splitter; *G*-Glan prism; *M*-magnet; *CL*-cylindrical lens; *T*-telescopic system; *D*- diaphragm; *L*- lens *PM*-parabolic mirror; *OMM*-optical-mechanical modulator; *P*-Teflon filter; *V*-Wollaston prism; *BD*-balanced detector.

THz radiation is focused by a parabolic second mirror *PM2* to the electro-optical crystal *CdTe*, with an area of $10 \times 10 \text{ mm}^2$ and a thickness of 2 mm. This crystal is the most suitable for the dispersion properties of electro-optic detection of THz radiation.

Femtosecond laser probe beam passes a Glan prism *G*, which makes the radiation horizontal linearly polarized with the accuracy of 10^{-4} . The next telescope *T* increases the diameter of the beam to about 5 mm, and the cylindrical lens *CL* focuses the radiation on the central region of the crystal *CdTe*. The radiation is formed to be rectangular with dimensions of $5 \times 1 \text{ mm}^2$. 5 mm dimension is in the direction of the horizontal axis *x*. When the probe beam propagates to the electro-optical crystal *CdTe*, it is exposed to a constant electric field of collinear propagating terahertz pulse, which affects the linear polarization of the probe beam to be changed to elliptical polarization. A quarter-wave plate $\lambda/4$ transforms the probe beam polarization to near-circular polarization. The beams with different polarization states are separated by a Wollaston prism *V* and they fall on the balanced detector *BD*. Since the magnitude of the birefringence is directly proportional to the electric field, the intensity difference on the photodiode balanced circuit is also proportional to the field of THz radiation. The signal from the balanced detector enters to the lock-in amplifier, consistent with the optical modulator *OMM* and then signal goes to an analog-to-digital converter built into *PC*.

The optical delay line changes the crossing time of terahertz radiation and the probe beam in the crystal. By variations in the delay, the effect of birefringence on the amplitude of the electric field of the terahertz pulse time $E_{\text{THz}}(t)$ can be recorded. The spectrum of the given signal is determined by Fourier

transformation, while the absorption spectrum is determined by subtracting the two spectra recorded when the THz pulse passes through a object and without it. Typical THz signals and their spectra are shown in Fig. 4.7.

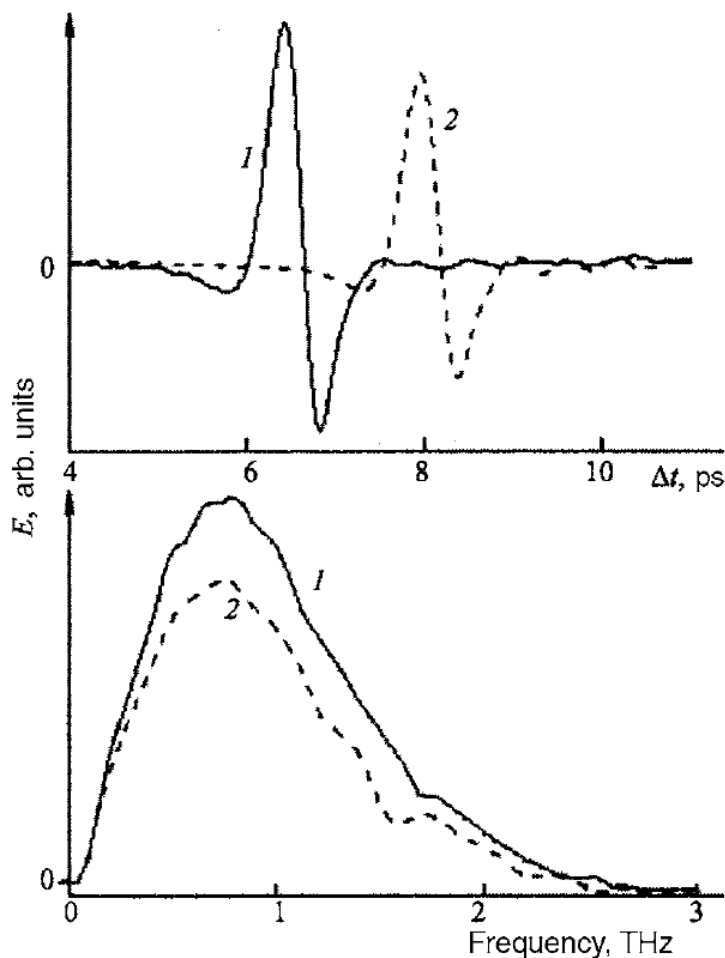


Fig. 4.7. Typical THz signals and their spectra, obtained by Fourier transforming the time form, before (1) and after (2) being transmitted through a sample

Based on the measured absorption spectra, various frequency resonances responsible for various vibrations of the molecules were determined, as well as the frequency dispersions of various isomers in the THz range. When the absorption spectra of the three isomers are compared, it becomes possible to determine the localization of the various vibrational modes in a complex molecule.

Thus, THz spectroscopy using ultrashort pulses opens up new possibilities of investigating the resonances of complex molecules, including biological molecules, in a wavelength range that had been inaccessible.

REFERENCES

1. R A. Lewis, "A review of terahertz sources," *J. Phys. D.-Appl Phys*, **47**: 374001 (2014)
2. T. Nagatsuma, G. Ducournau, and C. C. Renaud, "Advances in terahertz communications accelerated by photonics," *Nat. Photonics*, **10**, no. 6, pp. 371–379 (2016).

3. D. A. Newnham and P. F. Taday, "Pulsed terahertz attenuated total reflection spectroscopy," *Appl. Spectrosc.* **62**, 394 (2008).
4. N. V. Petrov, M. S. Kulya, A. N. Tsyppkin, V. G. Bespalov, A. Gorodetsky, "Application of terahertz pulse time-domain holography for phase imaging", *IEEE Trans. THz Sci. Technol.*, vol. 6, no. 3, pp. 464-472, May 2016.
5. M. C. Hoffmann, J. A. Fülöp, "Intense ultrashort terahertz pulses: Generation and applications," *J. Phys. D.-Appl. Phys.*, **44**: 083001 (2011)
6. D. H. Auston, "Picosecond optoelectronic switching and gating in silicon," *Appl. Phys. Lett.* **26**, 101 (1975).
7. V. G. Bespalov, V. N. Krylov, S. É. Putilin, and D. I. Stasel'ko, "Generating radiation in the far-IR region with femtosecond optical excitation of the semiconductor InAs in a magnetic field," *Opt. Spektrosk.* **93**, 158 (2002) (*Opt. Spectrosc.* **93**, 148 (2002)).
8. D. V. Seletskiy, "Efficient terahertz emission from InAs nanowires," *Phys. Rev. B - Condens. Matter Mater. Phys.* **84**. 115421 (2011)
9. J. Hebling, K.-L. Yeh, M. C. Hoffmann, B. Bartal, and K. A. Nelson, "Generation of high-power terahertz pulses by tilted-pulse-front excitation and their application possibilities," *J. Opt. Soc. Am. B* **25**, 6 (2008).
10. Y. Mori, Y. Takahashi, T. Iwai, M. Yoshimura, Y. Khin Yap, and T. Sasaki, "Slope nucleation method for the growth of high-quality 4-dimethylamino-methyl-4-stilbazolium-tosylate _DAST_ crystals," *Jpn. J. Appl. Phys.* **39**, L1006 (2000).
11. A. Schneider, M. Neis, M. Stillhart, B. Ruiz, R. U. A. Khan, and P. Gunter, "Generation of terahertz pulses through optical rectification in organic DAST crystals: theory and experiment," *J. Opt. Soc. Am. B* **23**, 1822 (2006).
12. A.G. Stepanov, J. Hebling, J. Kuhl, "Efficient generation of subpicosecond terahertz radiation by phase-matched optical rectification using ultrashort laser pulses with tilted pulse fronts," *Appl. Phys. Lett.* **83**(15), 3000 (2003).
13. D. J. Cook and R. M. Hochstrasser, "Intense terahertz pulses by four-wave rectification in air," *Opt. Lett.* **25**, 1210 (2000).
14. X. Xie, J. Xu, J. Dai, and X. C. Zhang, "Enhancement of terahertz wave generation from laser-induced plasma," *Appl. Phys. Lett.* **90**, 141104 (2007).
15. S. L. Chin, T. J. Wang, C. Marceau, J. Wu, J. S. Liu, O. Kosareva, N. Panov, Y. P. Chen, J. F. Daigle, S. Yuan, A. Azarm, W. W. Liu, T. Seideman, H. P. Zeng, M. Richardson, R. Li, and Z. Z. Xu, "Advances in Intense Femtosecond Laser Filamentation in Air," vol. 22, no. 1, pp. 1– 53, (2012).
16. E. Matsubara, M. Nagai, and M. Ashida, "Ultrabroadband coherent electric field from far infrared to 200 THz using air plasma induced by 10 fs pulses," *Appl. Phys. Lett.*, vol. 101, no. 1 (2012).
17. P. K. Benicewicz, J. P. Roberts, and A. J. Taylor, "Scaling of terahertz radiation from large-aperture biased photoconductors," *J. Opt. Soc. Am. B* **11**, 2533 (1994).

18. A. M. Zheltikov, "Let there be white light: supercontinuum generation by ultrashort laser pulses," *Usp. Fiz. Nauk* **176**, 623 _2006_ _Phys. Usp. **49**, 605 – 642 (2006).
19. B. I. Greene, P. N. Saeta, R. D. Douglas, and S. L. Chuang, "Far-infrared light generation at semiconductor surfaces and its spectroscopic applications," *Int. J. Quantum Chem.* **28**, 2302 (1992).
20. Zhang X.C., Xu J. Introduction to THz wave photonics. NY.: Springer, 2009. 246 P.
21. Lee, Yun-Shik. Principles of terahertz science and technology. Springer Science+Business Media, LLC, XII. 2009. 340 p.

Миссия университета – генерация передовых знаний, внедрение инновационных разработок и подготовка элитных кадров, способных действовать в условиях быстро меняющегося мира и обеспечивать опережающее развитие науки, технологий и других областей для содействия решению актуальных задач.

Образовательные программы

Факультет фотоники и оптоинформатики открывает дорогу в Университет ИТМО абитуриентам, которые увлечены миром голографии и лазеров, оптических компьютеров и квантового шифрования, нанобъектов и живых клеток, физики и биомедицины.

Фемтотехнологии фотоники и оптоинформатики (бакалавриат)

Цель программы — подготовка специалистов мирового уровня в области разработки и эксплуатации быстродействующих систем и устройств фотоники на основе фемтотехнологий.

Студенты, обучающиеся по этой программе, приобретают фундаментальные знания в области оптики и квантовой физики, в том числе физики взаимодействия интенсивного излучения сверхкороткой длительности с веществом в различных его состояниях. В период обучения студенты участвуют в реализации реальных проектов лабораторий Международного института фотоники и оптоинформатики и приобретают уникальный опыт применения на практике полученных фундаментальных знаний.

Биофотоника (магистратура)

Цель программы — подготовка специалистов мирового уровня в области разработки и эксплуатации быстродействующих систем и устройств фотоники, а также лазерно-оптических методов диагностики в медицине, биологии и системах безопасности на основе фемтотехнологий.

Студенты, обучающиеся по этой программе, приобретают фундаментальные знания в области оптической и квантовой физики, в том числе физики взаимодействия интенсивного излучения сверхкороткой длительности с веществом в различных его состояниях, биофотоники, оптической диагностики биомедицинских объектов.

Беспалов Виктор Георгиевич, Козлов Сергей Аркадьевич,
Путилин Сергей Эдуардович, Смолянская Ольга Алексеевна

Femtosecond optics and femtotechnologies.

учебно-методическое пособие

В авторской редакции

Редакционно-издательский отдел Университета ИТМО

Зав. РИО

Н.Ф. Гусарова

Подписано к печати

Заказ №

Тираж

Отпечатано на ризографе

Редакционно-издательский отдел
Университета ИТМО
197101, Санкт-Петербург, Кронверкский пр., 49